The Astrophysical Journal, 604:388–413, 2004 March 20

TOWARD A DETERMINISTIC MODEL OF PLANETARY FORMATION. I. A DESERT IN THE MASS AND SEMIMAJOR AXIS DISTRIBUTIONS OF EXTRASOLAR PLANETS

S. Ida
Tokyo Institute of Technology, Ookayama, Meguro-ku, Tokyo 152-8551, Japan; and
University of California Observatories, Lick Observatory, University of California,
Santa Cruz, CA 95064; ida@geo.titech.ac.jp

AND

D. N. C. Lin
University of California Observatories, Lick Observatory, University of California,
Santa Cruz, CA 95064; lin@ucolick.org
Received 2003 August 14; accepted 2003 December 1

ABSTRACT

In an attempt to develop a deterministic theory for planet formation, we examine the accretion of cores of giant planets from planetesimals, gas accretion onto the cores, and their orbital migration. We adopt a working model for nascent protostellar disks with a wide variety of surface density distributions in order to explore the range of diversity among extrasolar planetary systems. We evaluate the cores' mass growth rate $\dot{M}_c$ through runaway planetesimal accretion and oligarchic growth. The accretion rate of cores is estimated with a two-body approximation. In the inner regions of disks, the cores' eccentricity is effectively damped by their tidal interaction with the ambient disk gas and their early growth is stalled by "isolation." In the outer regions, the cores' growth rate is much smaller. If some cores can acquire more mass than a critical value of several Earth masses during the persistence of the disk gas, they would be able to rapidly accrete gas and evolve into gas giant planets. The gas accretion process is initially regulated by the Kelvin-Helmholtz contraction of the planets' gas envelope. Based on the assumption that the exponential decay of the disk gas mass occurs on the timescales $\sim 10^6$–10^7 yr and that the disk mass distribution is comparable to those inferred from the observations of circumstellar disks of T Tauri stars, we carry out simulations to predict the distributions of masses and semimajor axes of extrasolar planets. In disks as massive as the minimum-mass disk for the solar system, gas giants can form only slightly outside the "ice boundary" at a few AU. However, cores can rapidly grow above the critical mass inside the ice boundary in protostellar disks with 5 times more heavy elements than those of the minimum-mass disk. Thereafter, these massive cores accrete gas prior to its depletion and evolve into gas giants. The limited persistence of the disk gas and the decline in the stellar gravity prevent the formation of cores capable of efficient gas accretion outside 20–30 AU. Unimpeded dynamical accretion of gas is a runaway process that is terminated when the residual gas is depleted either globally or locally in the form of a gap in the vicinity of their orbits. Since planets' masses grow rapidly from 10 to 100 $M_\oplus$, the gas giant planets rarely form with asymptotic masses in this intermediate range. Our model predicts a paucity of extrasolar planets with mass in the range 10–100 $M_\oplus$ and semimajor axis less than 3 AU. We refer to this deficit as a "planet desert." We also examine the dynamical evolution of protoplanets by considering the effect of orbital migration of giant planets due to their tidal interactions with the gas disks, after they have opened up gaps in the disks. The effect of migration is to sharpen the boundaries and to enhance the contrast of the planet desert. It also clarifies the separation between the three populations of rocky, gas giant, and ice giant planets. Based on our results, we suggest that the planets' mass versus semimajor axes diagram can provide strong constraints on the dominant formation processes of planets analogous to the implications of the color-magnitude diagram on the paths of stellar evolution. We show that the mass and semimajor axis distributions generated in our simulations for the gas giants are consistent with those of the known extrasolar planets. Our results also indicate that a large fraction (90%–95%) of the planets that have migrated to within 0.05 AU must have perished. Future observations can determine the existence and the boundaries of the planet desert in this diagram, which can be used to extrapolate the ubiquity of rocky planets around nearby stars. Finally, the long-term dynamical interaction between planets of various masses can lead to both eccentricity excitation and scattering of planets to large semimajor axes. These effects are to be included in future models.

Subject headings: planets and satellites: formation — solar system: formation — stars: statistics

On-line material: color figures

1. INTRODUCTION

More than 100 extrasolar planets have been discovered so far. This sample is sufficiently large that some clues and constraints on the formation of extrasolar planets may be inferred from their kinematic properties. Figure 1 shows the distributions of semimajor axes (a) and masses (M_p) of the known extrasolar planets as of 2003 July.[1] Various radial velocity surveys may have exhaustively found most of the planets in the solar neighborhood with radial velocity amplitude $v_r \gtrsim 10\ \mathrm{m\ s^{-1}}$

[1] The Extrasolar Planets Encyclopedia is available at http://www.obspm.fr/encycl/encycl.html.

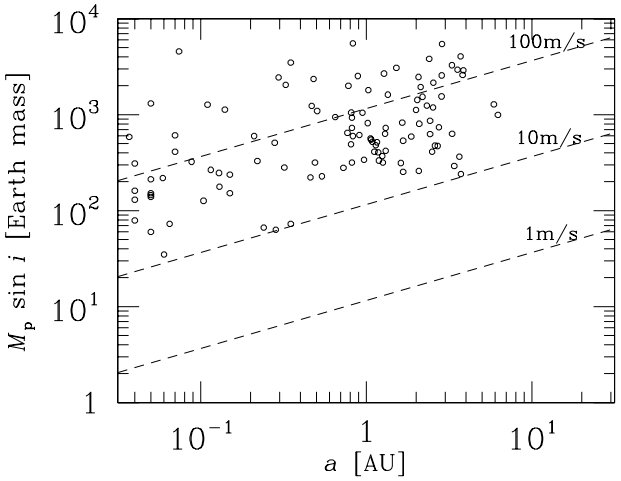

FIG. 1.—Distributions of semimajor axes (a) and masses (M_p) of discovered extrasolar planets (*open circles*). Unit of mass is Earth mass $M_\oplus$ (Jupiter mass is $M_J \simeq 320\ M_\oplus$). Here i is the angle between an orbital plane and the line of sight. The dashed ascending lines correspond to radial velocity amplitude of 100, 10, and 1 m s^{-1} (assuming that the host star mass is 1 $M_\odot$).

and relatively small semimajor axes, $a \lesssim 4-5$ AU, which correspond to orbital periods $\lesssim$10 yr. The mass distribution in these regions appears to follow a weak power-law function in M_p with an abrupt upper cutoff at around $10M_J$ (Jorissen, Mayor, & Udry 2001; Tabachnik & Tremaine 2002; Zucker & Mazeh 2002), where M_J is a Jupiter mass and is $\simeq$320 $M_\oplus$ ($M_\oplus$ is an Earth mass).

However, Figure 1 also shows a correlation between the M_p and a distributions. Zucker & Mazeh (2002), Patzold & Rauer (2002), and Udry, Mayor, & Santos (2003) discussed a deficit of massive ($M_p \gtrsim 5M_J$) and short-period ($a \lesssim 0.2$ AU) planets. Here we focus on another domain of paucity in the M_p-a distribution: the regions $a \gtrsim 0.2$ AU and $M_p \lesssim M_J$ (Fig. 1). This paucity is not due to the observational selection effects of precision and legacy baseline since planets in this domain have $v_r \gtrsim 10$ m s^{-1} and orbital periods P less than a few years (Udry et al. 2003). In this paper we suggest that this paucity reflects the condition for and the process of planetary formation.

We interpret the observational data on Jupiter-mass extrasolar planets with the conventional core accretion model of gas giant planets (Wuchterl, Guillot, & Lissauer 2000 and references therein). In the standard model, terrestrial planets and solid cores of gas giants are formed through the coagulation of planetesimals with initial sizes $\sim$1–10 km (e.g., Safronov 1969; Wetherill 1980; Hayashi, Nakazawa, & Nakagawa 1985). Cores that are heavier than a few lunar masses attract the disk gas and form hydrostatic atmospheres. However, if a solid core reaches a critical mass of greater than or approximately several $M_\oplus$ (§ 3.1), the pressure gradient in the planet's gaseous atmosphere can no longer support against its gravity and the planet's atmosphere collapses onto its core (Mizuno 1980; Bodenheimer & Pollack 1986; Pollack et al. 1996; Ikoma, Nakazawa, & Emori 2000). Subsequent disk gas accretion onto the solid core forms a gas giant planet.

The cores' asymptotic masses and their accretion timescales are determined by surface density of the planetesimal swarm and orbital radius (Kokubo & Ida 2002). In general, the formation of the gas giants is favored slightly outside the "ice boundary" at a few AU (Kokubo & Ida 2002), where the surface density of dust particles increases by a factor of 3–4 as ice condenses. This enhancement of the dust surface density facilitates the formation of large cores. Well beyond the "ice boundary" ($\gtrsim$10 AU), the cores' growth rate is so small that the residual gas in the disk tends to be depleted before it can be accreted. In very massive protoplanetary disks, however, cores can reach the critical mass inside the ice boundary (Lin & Ida 1997; Kokubo & Ida 2002). Since the core accretion is relatively fast in the inner regions of the disk, gas accretion onto cores can start well before the gas is depleted. Unimpeded dynamical accretion of gas is a runaway process that is terminated when the residual gas is depleted either globally or locally in the form of a gap in the vicinity of the gas giants' orbits. However, prior to a self-limiting growth stage, the planets grow so rapidly from 10 to more than 100 $M_\oplus$ that they rarely emerge with an asymptotic mass in the intermediate range (10–100 $M_\oplus$). We refer to such a planet-deficit domain in the M_p-versus-a distribution as a "planet desert."

After their formation, gas giant planets with sufficiently large masses to open up gaps also undergo type II orbital migration, which is well coupled to the viscous evolution of their nascent disks (Lin & Papaloizou 1985). If these planets' tidal and magnetospheric interaction with their host stars can halt their inward migration, there would be an accumulation of "short-period planets" (equivalently "close-in planets" or "hot Jupiters"), near the disk inner edge ($\lesssim$0.1 AU). Dozens of short-period planets have been discovered (Marcy, Cochran, & Mayor 2000), and their masses appear to be relatively small (Udry et al. 2003). These planets have either formed with relatively low masses (see § 4) or lost some of their initial mass through Roche lobe overflow (Trilling et al. 1998; Gu, Lin, & Bodenheimer 2003). The latter process is only effective in the regions close to the stellar surface. Massive short-period planets may also be more vulnerable to postformation orbital decay as a result of their enhanced tidal interaction with their host stars (Zucker & Mazeh 2002; Patzold & Rauer 2002).

Gas giant planets may attain a in the range of 0.2–3 AU, only if the disk gas is timely depleted during their migration (Trilling, Lunine, & Benz 2002; Armitage et al. 2002). Type II migration proceeds at a faster pace for planets with relatively lower mass and smaller orbital radius. As shown in § 5, the intermediate-mass planets can open up gaps in inner regions ($a \lesssim 1$ AU) and easily migrate to the proximity of the host stars. Larger planets tend to migrate less rapidly than the intermediate-mass planets.

Intermediate-mass planets with insufficient masses to open gaps also interact tidally with the disk gas through their Lindblad and corotation resonances (Goldreich & Tremaine 1980). In principle, any imbalance in the torque can lead to "type I" migration (Ward 1986). The effect of the corotation resonances (Tanaka, Takeuchi, & Ward 2002; Bate et al. 2003) and secondary instabilities in the vicinity of the co-orbital region (Balmforth & Korycansky 2001; Koller, Li, & Lin 2003) may be able to quench the magnitude and sign of the net torque. Observationally, there is no evidence that type I migration has brought in any water-filled terrestrial planets into the inner solar system.

Well outside the ice boundary ($\gtrsim$3 AU), the intermediate-mass planets can slowly accrete nearby planetesimals. Prior to the depletion of the gas, however, intermediate-mass planets are unable to open up gaps in outer regions. In the absence of type I migration, they cannot migrate to the inner region from larger orbital radii. Cores in the outer regions of the disk can attain masses in excess of 1 $M_\oplus$ after the gas depletion (§ 2).

The mass distributions for long-period planets are expected to be continuous. However, with the residual gas depleted, the intermediate-mass planets that formed lately cannot migrate to fill the planet desert.

Based on these considerations, we suggest that the intermediate-mass planets may be rare and their deficit gives rise to a "planet desert" at 0.2–3 AU. In § 2 we present the model of core accretion and predict cores' masses as functions of their nascent disks' mass and semimajor axis. In § 3 we include the effects of gas accretion onto the cores. Assuming an appropriate distribution of disk masses that may be comparable to the observationally inferred mass distribution, we carry out, in § 4, Monte Carlo calculations to simulate the mass and semimajor axis distributions of extrasolar planets. The predicted distributions clearly show a paucity of planets with masses $\sim$10–100 $M_\oplus$ at $a \lesssim 3$ AU. In § 5 we discuss the effects of radial migration of giant planets due to their tidal interaction with a gas disk. We show that type II migration sharpens the boundaries and enhances the contrast of the planet desert. In § 6 we summarize our results.

2. CORE ACCRETION

In this section we briefly recapitulate the current theories for solid core accretion. Our main objective is to determine the cores' growth rate and asymptotic masses.

2.1. *Core Accretion Model: The Feeding Zone*

In an early stage of planetesimal accretion, the largest planetesimals have the shortest mass-doubling timescale. This process is commonly referred to as the "runaway growth" (e.g., Greenberg et al. 1978; Wetherill & Stewart 1989; Aarseth, Lin, & Palmer 1993; Kokubo & Ida 1996). In the limit that their velocity dispersion is relatively small, field planetesimals are readily captured by nearby runaway bodies (cores). However, the differential Keplerian speed of the planetesimals prevents them from reaching the distant runaway cores until they have acquired sufficient orbital eccentricity. The region within which the runaway cores can directly accrete planetesimals is commonly referred to as the "feeding zone." When the runaway cores capture all the planetesimals in their feeding zones, their growth stops as they acquire an "isolation mass." Lissauer (1987) evaluated the isolation mass as a function of the initial surface density of the solid components in protostellar disks. Assuming a negligible velocity dispersion for the planetesimals, the full width of the feeding zone is given by $\Delta a_c \simeq 2(12)^{1/2} r_{\rm H} \simeq 7 r_{\rm H}$, where

$$r_{\rm H} \equiv \left(\frac{M_c}{3M_*}\right)^{1/3} a \tag{1}$$

is the Hill radius (Roche lobe radius) for a solid core with a mass M_c around a host star with a mass M_*.

However, when a core becomes sufficiently massive to excite the eccentricity and to pump up velocity dispersion of the neighboring planetesimals, its feeding zone expands. The increases in the relative speed between the planetesimals and the cores also reduce the effective cross section of the cores such that their growth slows down (Ida & Makino 1993; Aarseth et al. 1993; Rafikov 2003). The relatively massive cores are more effective in stirring up the velocity dispersion of their neighbors so that the reduction of their effective cross section is larger. Consequently, the growth timescale becomes an increasing function of the cores' mass. Such a self-regulated growth results in the formation of a population of comparable-mass cores that are embedded in a swarm of small and relatively eccentric planetesimals (Kokubo & Ida 1998, 2000; Thommes, Duncan, & Levison 2003). In this system, the orbital spacings of the cores (equivalently, full width of their feeding zone, Δa_c) are nearly equal to one another and are as large as $\sim 10 r_{\rm H}$. This maximization of spacing is the combined consequence of the distant perturbations between the cores and the effect of dynamical friction from the small planetesimals on the cores (Kokubo & Ida 1995). Kokubo & Ida (1998) called this coagulation process the "oligarchic growth." Because the width of the feeding zone is

$$\Delta a_c \sim 10 r_{\rm H} \tag{2}$$

during the oligarchic growth stage, the isolation masses are slightly larger than those estimated by Lissauer (1987).

The concept of an isolation mass induced by the depletion of the feeding zone is based on the assumption that the orbits of the cores do not evolve with time. In reality, the cores undergo radial diffusion due to their scattering of the field planetesimals (e.g., Murray et al. 1998; Ida et al. 2000) and their tidal interaction with the gas disk (type I migration; e.g., Goldreich & Tremaine 1980; Ward 1986). Under the action of gas drag, the small planetesimals and dust particles may also undergo migration (e.g., Adachi, Hayashi, & Nakazawa 1976). These effects can lead to an expansion of the feeding zones. Thus, in a prescription for the asymptotic mass of cores' growth, it is worthwhile to consider the possibility that the cores' feeding zone may be extended throughout the disk.

2.2. *The Cores' Growth Rate*

The growth rate of the cores is determined by the velocity dispersion (σ) or equivalently the eccentricity distribution of the planetesimals and cores. Eccentricity damping due to their tidal interaction with the disk gas (Artymowicz 1993; Ward 1993) inhibits the cores from attaining any significant growth in their velocity dispersion. In contrast, the eccentricity of the low-mass planetesimals is less effectively damped. Instead, it is excited by cores through recoil of dynamical friction. Through a series of three-dimensional numerical simulations, Kokubo & Ida (2002) showed that the planetesimals' eccentricity is larger than the ratio of the cores' $r_{\rm H}$ and their semimajor axes so that the cores' growth timescale is well described by a simple two-body approximation.

In the modest to high-σ limit, the cores' accretion rate at an orbital radius a is (Safronov 1969)

$$\begin{aligned}\dot{M}_c &\sim \pi R_c^2 \rho_d \left(\frac{2GM_c}{R_c\sigma^2}\right)\sigma \sim 2\pi R_c^2 \Sigma_d \Omega_{\rm K}\left(\frac{GM_c}{R_c\sigma^2}\right) \\ &\sim 2\pi\left(\frac{R_c}{a}\right)\left(\frac{M_c}{M_*}\right)\left(\frac{a\Omega_{\rm K}}{\sigma}\right)^2 \Sigma_d a^2 \Omega_{\rm K},\end{aligned} \tag{3}$$

where $\Omega_{\rm K} = (GM_*/a^3)^{1/2}$ is a Kepler frequency, ρ_d and Σ_d are the spatial and surface density of solid components ($\rho_d \sim \Sigma_d \Omega_{\rm K}/\sigma$), respectively, and R_c is a physical radius of the core. In order for the planetesimals within Δa_c to reach the cores,

$$\frac{\sigma}{\Omega_{\rm K}} \sim \Delta a_c \sim 10\left(\frac{M_c}{3M_*}\right)^{1/3} a, \tag{4}$$

so that the solid cores' accretion timescale is

$$\tau_{c,\mathrm{acc}} = \frac{M_c}{\dot{M}_c} \sim \left(\frac{a}{R_c}\right)\left(\frac{M_c}{\Sigma_d a^2}\right)\left(\frac{M_c}{M_*}\right)^{-1/3} T_{\mathrm{K}}, \quad (5)$$

where $T_{\mathrm{K}} = 2\pi/\Omega_{\mathrm{K}}$ $[=(M_*/M_\odot)^{-1/2}(a/1\ \mathrm{AU})^{3/2}\ \mathrm{yr}]$ is the Kepler period. By taking into account the effect of gas drag on the planetesimals' velocity dispersion, Kokubo & Ida (2002) derived a more detailed expression (see their eqs. [15] and [16]),

$$\tau_{c,\mathrm{acc}} \simeq 1.2 \times 10^5 \left(\frac{\Sigma_d}{10\ \mathrm{g\ cm^{-2}}}\right)^{-1}\left(\frac{a}{1\ \mathrm{AU}}\right)^{1/2}\left(\frac{M_c}{M_\oplus}\right)^{1/3} \times \left(\frac{M_*}{M_\odot}\right)^{-1/6}\left[\left(\frac{\Sigma_g}{2.4 \times 10^3\ \mathrm{g\ cm^{-2}}}\right)^{-1/5} \times \left(\frac{a}{1\ \mathrm{AU}}\right)^{1/20}\left(\frac{m}{10^{18}\ \mathrm{g}}\right)^{1/15}\right]^2 \mathrm{yr}, \quad (6)$$

where Σ_g is the surface density of the gas in the disk, m is the mass of typical planetesimals, and $M_\odot$ is the Sun's mass. Since $\tau_{c,\mathrm{acc}} \equiv M_c/\dot{M}_c$, we find from equation (6)

$$M_c(t) \simeq \left(\frac{t}{3.5 \times 10^5\ \mathrm{yr}}\right)^3\left(\frac{\Sigma_d}{10\ \mathrm{g\ cm^{-2}}}\right)^3 \times \left(\frac{\Sigma_g}{2.4 \times 10^3\ \mathrm{g\ cm^{-2}}}\right)^{6/5}\left(\frac{m}{10^{18}\ \mathrm{g}}\right)^{-2/5} \times \left(\frac{a}{1\ \mathrm{AU}}\right)^{-9/5}\left(\frac{M_*}{M_\odot}\right)^{1/2} M_\oplus, \quad (7)$$

where we neglect variations of Σ_d and Σ_g with time. This approximation is adequately satisfied in the inner regions of the disk where $\tau_{c,\mathrm{acc}}$ is small compared with the gas depletion timescale.

In the outer regions of the disk, the rate of mass growth is reduced from the above expression during the depletion of the disk gas. In equation (48), we introduce a prescription for the global depletion of the gas. For this prescription of Σ_g, the evolution of the core mass becomes

$$M_c(t) \simeq \left(\frac{\tau_{\mathrm{disk}}}{1.4 \times 10^5\ \mathrm{yr}}\right)^3\left(\frac{\Sigma_d}{10\ \mathrm{g\ cm^{-2}}}\right)^3 \times \left(\frac{\Sigma_{g,0}}{2.4 \times 10^3\ \mathrm{g\ cm^{-2}}}\right)^{6/5}\left(\frac{m}{10^{18}\ \mathrm{g}}\right)^{-2/5} \times \left(\frac{a}{1\ \mathrm{AU}}\right)^{-9/5}\left(\frac{M_*}{M_\odot}\right)^{1/2}\left[1 - \exp\left(\frac{-2t}{5\tau_{\mathrm{disk}}}\right)^3\right] M_\oplus, \quad (8)$$

where τ_{disk} is the disk depletion timescale. In the limit of $t \ll \tau_{\mathrm{disk}}$, equation (8) reduces to equation (7). In principle, the magnitude of $\tau_{c,\mathrm{acc}}$ in the inner disk may be reduced by the core's inward type I migration (Tanaka & Ida 1999; Papaloizou & Terquem 1999). However, the long $\tau_{c,\mathrm{acc}}$ is a growth barrier in the outer regions of the disk.

According to equation (8), the cores attain an asymptotic mass. But for $t > \tau_{\mathrm{disk}}$, the assumptions for circular orbits of the cores and damping of planetesimals' σ by gas drag break down. When all the gas is depleted and all the heavy-elemental content is retained by the oligarchic cores, their σ increases to become comparable to their characteristic surface speed $\sigma \sim V_{\mathrm{surf}} = (GM_c/R_c)^{1/2}$ and their collisional cross section reduces to their physical cross section. In this limit, the growth timescale for the final planetary embryos becomes

$$\tau_{e,\mathrm{acc}} \sim \left(\frac{a}{R_e}\right)^2\left(\frac{M_e}{\Sigma_e a^2}\right)\left(\frac{T_{\mathrm{K}}}{2\pi^2}\right) \sim 2 \times 10^7 \left(\frac{\Sigma_d}{10\ \mathrm{g\ cm^{-2}}}\right)^{-1}\left(\frac{M_{\mathrm{e}}}{M_\oplus}\right)^{1/3}\left(\frac{\rho_{\mathrm{e}}}{1\ \mathrm{g\ cm^{-3}}}\right)^{2/3} \times \left(\frac{M_*}{M_\odot}\right)^{-1/2}\left(\frac{a}{1\ \mathrm{AU}}\right)^{3/2} \mathrm{yr}, \quad (9)$$

where M_e, R_e, and ρ_e are a mass, radius, and an internal density of the embryo, respectively. Here we refer to solid planets after depletion of the gas as "embryos" rather than "cores." The reduced collisional cross section significantly lengthens the growth timescale for the embryos from that of the cores. The corresponding mass for the embryos is

$$M_e(t) \simeq M_e(\tau_{\mathrm{disk}}) + \left(\frac{t - \tau_{\mathrm{disk}}}{6 \times 10^7\ \mathrm{yr}}\right)^3\left(\frac{\Sigma_d}{10\ \mathrm{g\ cm^{-2}}}\right)^3 \times \left(\frac{\rho_{\mathrm{e}}}{1\ \mathrm{g\ cm^{-3}}}\right)^{-2}\left(\frac{a}{1\ \mathrm{AU}}\right)^{-9/2} M_\oplus. \quad (10)$$

2.3. *Disk Structure Models: The Temperature and Surface Density Distributions*

The cores and embryos' mass, as expressed in both equations (8) and (10), is a function of the surface density of the heavy elements in the form of condensed grains and planetesimals, Σ_d. The distribution of Σ_d is poorly determined theoretically and observationally. In principle, the Σ_d distribution is determined by the infall pattern of the heavy elements, the condensation, growth, and sublimation rates of grains, and the particles' interaction with ambient disk gas. Here we adopt an ad hoc power-law distribution such that

$$\Sigma_d = f_d \eta_{\mathrm{ice}} \times 10\left(\frac{a}{1\ \mathrm{AU}}\right)^{-3/2} \mathrm{g\ cm^{-2}}, \quad (11)$$

based on a phenomenological minimum-mass solar nebula model (Hayashi 1981). The power-law dependence may be the consequence of self-similar evolution. We use this prescription as a fiducial model. We plot Σ_d as a function of a for $f_d = 0.1$, 1, and 10 in Figure 2. Using these models, we assess the formation properties of planetary systems as a function of Σ_d. The step function variable η_{ice} is introduced to express the effect of ice condensation/sublimation across the ice boundary ($a_{\mathrm{ice}} \sim$ a few AU; see eq. [15]). For the inner disk with $a < a_{\mathrm{ice}}$, $\eta_{\mathrm{ice}} = 1$, and for outer regions with $a > a_{\mathrm{ice}}$, $\eta_{\mathrm{ice}} \sim 3$–4. Following the minimum-mass solar nebula model, we adopt $\eta_{\mathrm{ice}} = 4.2$ to represent the solar abundance distribution (Hayashi 1981).

We also introduce a scaling parameter for the total disk mass, f_d, which is assumed to be a constant parameter throughout the disk. In the case of the minimum-mass disk model for the solar system (Hayashi 1981), the scaling parameter $f_d \simeq 0.7$. This value would be larger if the formation of

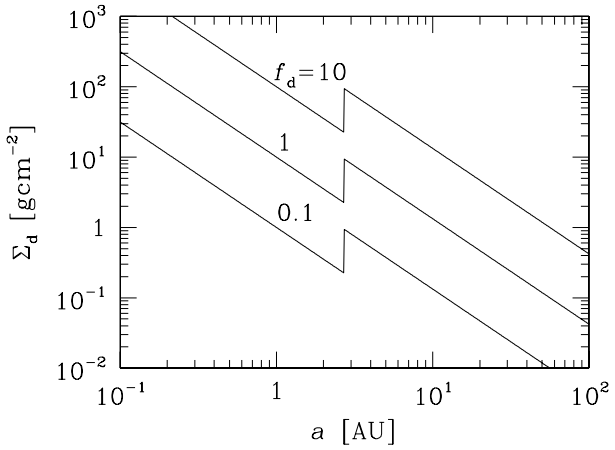

FIG. 2.—Σ_d as a function of a that we used. Here f_d is an enhancement factor from the minimum-mass disk model for our solar system. The jumps at 2.7 AU are caused by ice grain condensation at $a > 2.7$ AU.

the solid cores and their retention into the solar system planets were not highly efficient. Radio observations of the continuum radiation in the millimeter-wave length range measure the dust emission from the disks. The observationally inferred total mass of dust, M_d, in the protostellar disks around classical T Tauri stars ranges from 10^{-5} to 3×10^{-3} $M_\odot$ (e.g., Beckwith & Sargent 1996). The disk mass determinations are somewhat uncertain as a result of the poorly known radiative properties of the grains. Nevertheless, their differential dust content provides reasonable evidence for a greater than an orders-of-magnitude dispersion in M_d. In addition, the image of the disks is not well resolved in many cases. A rough magnitude of f_d can be inferred from the total mass of the disk under the assumption that all disks have similar sizes (a few tens to 100 AU). The observationally inferred mass of T Tauri disks corresponds to a range of $f_d \sim 0.1$–30. We note that disks with f_d substantially larger than unity do commonly exist.

The presence of gas affects the velocity dispersion and therefore the growth rate of the cores. It is also important for the formation of gaseous giant planets. In principle, the magnitude of the gas surface density Σ_g is determined by the gas infall rate and it evolves as a consequence of the viscous stress in the disk (e.g., Lin & Papaloizou 1985). Similar to all astrophysical accretion disks, the effective viscosity is generally assumed to be due to turbulence. However, in regions of protostellar disks where planets emerge, the cause of turbulence is highly uncertain (Papaloizou & Lin 1995). For computational simplicity, we also assume that Σ_g has a similar power-law dependence on a as Σ_d such that

$$\Sigma_g = f_g\left(2.4 \times 10^3\right)\left(\frac{a}{1\ \mathrm{AU}}\right)^{-3/2}\ \mathrm{g\ cm^{-2}}. \qquad (12)$$

We vary the scaling parameter f_g to obtain different disk models and to test the dependence of the planetary properties on the mass of the gas disk. This assumption implies that the relative ratio of gas (volatiles) to dust (refractories composed mainly of heavy elements)

$$\frac{\Sigma_g}{\Sigma_d} = \frac{f_g}{f_d}\frac{240}{\eta_{\mathrm{ice}}} \qquad (13)$$

is uniform throughout the disk except across the discontinuity at the ice boundary. While $f_d/f_g = 1$ would represent the solar abundance, a different choice of f_d/f_g would represent the relative enrichment/depletion of the heavy elements in the disks.

In the above equations, we introduce a separate mass scaling parameter f_g for the gas in order to consider the possibility that the solid components may evolve independently from the gas. The basic concept of the minimum-mass solar nebula model is based on the assumption that all the heavy elements are retained while the original disk gas was depleted. Theories suggest that gas diffuses under the action of viscous stress, but dust and planetesimals migrate under the influence of the gas drag effect such that they tend to evolve independently from each other. Gas may also be preferentially depleted through the photoevaporation (e.g., Shu, Johnstone, & Hollenbach 1993; Matsuyama, Johnstone, & Murray 2003) and winds, while dusty grains may be preferentially retained by the disk (Shang et al. 2000).

At the moment, we can observe the dust component around most, as well as molecular hydrogen around a few, young stars. Among the classical T Tauri stars, there is no apparent dependence of the mass of the dust disks on the host stars' ages. For stars with ages greater than $\sim 10^6$–10^7 yr, the dust mass inferred from the millimeter-wave length continuum is much reduced (Beckwith & Sargent 1996; Wyatt et al. 2003). The near-IR signatures of disks also evolve on a similar timescale (Haisch, Lada, & Lada 2001). This decline has been interpreted as evidence for dust growth and planetesimal formation rather than the depletion of heavy elements (D'Alessio, Calvet, & Hartmann 2001). In this paper we adopt the conjecture that the surface density distribution of the dust plus planetesimals does not change except in those regions where they have been totally accreted by the cores.

Very little information is available on the evolution of Σ_g and f_g, but there is no indication of a divergent depletion pattern between molecular hydrogen and millimeter-size dust emission (Thi et al. 2001). In addition, the presence of spectral evidences and UV veiling for ongoing accretion is well correlated with the millimeter flux for the classical T Tauri stars. Both signatures of protostellar disks also disappear together among weak-line T Tauri stars (Duvert et al. 2000). Based on these observations, we adopt the most simple-minded assumption that gas is depleted on a similar timescale even though the gas and dust depletions proceed through different mechanisms.

In equation (11) we introduce a parameter η_{ice} to take into account the possibility of ice condensation. In order to determine the radius of the ice condensation, a_{ice}, we need to specify the gas temperature in the disk. In most planet-forming regions of interest, the gas density is sufficiently large to maintain a thermal coupling between the gas and the dust particles. In the optically thin regions of the disk, the dust and the gas are heated to an equilibrium temperature (Hayashi 1981) such that

$$T = 280\left(\frac{a}{1\ \mathrm{AU}}\right)^{-1/2}\left(\frac{L_*}{L_\odot}\right)^{1/4}\ \mathrm{K}$$
$$\simeq 280\left(\frac{a}{1\ \mathrm{AU}}\right)^{-1/2}\left(\frac{M_*}{M_\odot}\right)\ \mathrm{K}. \qquad (14)$$

For solar-type stars, the stellar luminosity L_* is roughly proportional to M_*^4. Since a_{ice} corresponds to the radius where $T \simeq 170$ K, we find that

$$a_{\rm ice} = 2.7\left(\frac{M_*}{M_\odot}\right)^2 \ {\rm AU}. \tag{15}$$

Hereafter we adopt $a_{\rm ice} = 2.7$ AU ($L_* = L_\odot$) until § 4.1. In the Monte Carlo calculations in §§ 4.2 and 5, we consider variation of $a_{\rm ice}$. Since scale height of a gas disk is $h \simeq c_s/\Omega_{\rm K}$, where c_s is sound velocity, from equation (14) we find

$$\frac{h}{a} = 0.05\left(\frac{a}{1\ {\rm AU}}\right)^{1/4}. \tag{16}$$

2.4. *The Cores' Asymptotic Mass*

Based on the distributions of Σ_d given by equation (11), we find from equation (7)

$$M_c(t) \simeq \left(\frac{t}{3.5\times 10^5\ {\rm yr}}\right)^3 \eta_{\rm ice}^3 f_d^3 f_g^{6/5} \times \left(\frac{a}{1\ {\rm AU}}\right)^{-81/10}\left(\frac{M_*}{M_\odot}\right)^{1/2} M_\oplus, \tag{17}$$

by assuming $m = 10^{18}$ g. Equivalently, the core accretion timescale is (eq. [6])

$$\tau_{c,\,\rm acc} \simeq 1.2\times 10^5 \eta_{\rm ice}^{-1} f_d^{-1} f_g^{-2/5}\left(\frac{a}{1\ {\rm AU}}\right)^{27/10} \times \left(\frac{M_c}{M_\oplus}\right)^{1/3}\left(\frac{M_*}{M_\odot}\right)^{-1/6} {\rm yr}. \tag{18}$$

Note that the actual timescale to reach M_c is $3\tau_{c,\,\rm acc}$ but not $\tau_{c,\,\rm acc}$. The numerical factor of 3 comes from the dependence that $\tau_{c,\,\rm acc} \propto M_c^{1/3}$.

The unimpeded core growth that is described by equation (17) cannot be sustained indefinitely. In the limit that damping effect due to disk-planet interaction (Artymowicz 1993; Ward 1993) regulates a small velocity dispersion for the cores, their growth terminates when they consume all the planetesimals in their feeding zones. If the radial diffusion/migration of the cores is neglected, the isolation mass (Lissauer 1987; Kokubo & Ida 1998, 2000)

$$M_{c,\,\rm iso} = 2\pi a \Delta a_c \Sigma_d \tag{19}$$

represents the asymptotic mass of the cores prior to the depletion of the disk gas. If we adopt $\Delta a_c = 10 r_{\rm H}$ (where M_c in $r_{\rm H}$ is replaced by $M_{c,\,\rm iso}$), the isolation mass would be

$$M_{c,\,\rm iso} \simeq 0.16\left(\frac{\Sigma_d}{10\ {\rm g\ cm^{-2}}}\right)^{3/2}\left(\frac{a}{1\ {\rm AU}}\right)^3 \times \left(\frac{\Delta a_c}{10 r_{\rm H}}\right)^{3/2}\left(\frac{M_*}{M_\odot}\right)^{-1/2} M_\oplus. \tag{20}$$

Upon acquiring $M_{c,\,\rm iso}$, the cores consume all the nearby planetesimals. These cores cannot cross each other's orbits, until the gaseous disk mass has decreased to $\lesssim 10^{-5}\ M_\odot$, equivalently $f_g \lesssim 10^{-3}$, and the damping effect due to disk-planet interaction becomes weak enough (Iwasaki et al. 2002; Kominami & Ida 2002). Even in a gas-free environment, a swarm of planetesimals has a tendency to evolve into a quasi-static oligarchic state. Kokubo & Ida (2002) performed three-dimensional N-body (with $N = 10,000$) simulations of planetesimal accretion in gas-free disks with a wide variety of surface density distribution of the planetesimal swarm. Their results indicate that the process of planetary accretion is fully consistent with the oligarchic growth scenario, i.e., the cores initially emerge with a characteristic orbital separation of $\Delta a_c \sim 10 r_{\rm H}$. In later stages, however, Δa_c increases to $\sim 15 r_{\rm H}$, which may be due to the radial diffusion of the cores (they neglected radial migration due to disk-planet interaction and did not include the effect of gas drag on a population of small planetesimals). Here we adopt $\Delta a_c = 10 r_{\rm H}$. From equation (11), we estimate the core masses in protoplanetary systems with equation (20) such that

$$M_{c,\,\rm iso} \simeq 0.16 \eta_{\rm ice}^{3/2} f_d^{3/2}\left(\frac{a}{1\ {\rm AU}}\right)^{3/4}\left(\frac{M_*}{M_\odot}\right)^{-1/2} M_\oplus. \tag{21}$$

If the effect of radial diffusion/migration of the cores is included, the final core mass could become larger than $M_{c,\,\rm iso}$. In the limiting case that a migrating core can acquire all the planetesimals inside its orbital semimajor axis, it would attain a maximum asymptotic mass

$$M_{c,\,\rm no\ iso} \sim \pi a^2 \Sigma_d \simeq 1.2\left(\frac{\Sigma_d}{10\ {\rm g\ cm^{-2}}}\right)\left(\frac{a}{1\ {\rm AU}}\right)^2 M_\oplus. \tag{22}$$

Based on the distributions of Σ_d given by equation (11), we find

$$M_{c,\,\rm no\ iso} \simeq 1.2 \eta_{\rm ice} f_d \left(\frac{a}{1\ {\rm AU}}\right)^{1/2} M_\oplus. \tag{23}$$

Growth beyond isolation is also possible after the gas depletion and the elimination of its damping effects (Iwasaki et al. 2002; Kominami & Ida 2002). After the gas depletion, the velocity dispersion of the residual cores grows until they cross each other's orbit. The final stages of cores' growth may proceed through giant impacts (Lissauer & Stewart 1993). Eventually a few surviving embryos acquire most of the residual planetesimals and less massive cores during the late oligarchic growth stage. Since their collisional cross section is reduced to their geometrical surface, the mass of the embryos evolves with the growth rate given by equation (9),

$$\frac{dM_e}{dt} = \frac{M_e}{\tau_{e,\,\rm acc}},$$

$$\tau_{e,\,\rm acc} \simeq 2\times 10^7 \eta_{\rm ice}^{-1} f_d^{-1}\left(\frac{a}{1\ {\rm AU}}\right)^3\left(\frac{M_{\rm e}}{M_\oplus}\right)^{1/3} \times \left(\frac{\rho_e}{1\ {\rm g\ cm^{-3}}}\right)^{2/3}\left(\frac{M_*}{M_\odot}\right)^{-1/2} {\rm yr}. \tag{24}$$

The asymptotic embryos' masses are given by equation (20) with $\Delta a_c \sim V_{\rm surf}/\Omega_{\rm K}$,

$$M_{e,\,\rm iso} \simeq 0.52 \eta_{\rm ice}^{3/2} f_d^{3/2}\left(\frac{a}{1\ {\rm AU}}\right)^{3/2}\left(\frac{M_*}{M_\odot}\right)^{-3/4} \times \left(\frac{\rho_e}{1\ {\rm g\ cm^{-3}}}\right)^{1/4} M_\oplus. \tag{25}$$

Such a scenario is consistent with the current model for the origin of the Moon (Hartmann & Davis 1975; Cameron & Ward 1976) and the apparently young isotropic age of the Earth, in comparison with asteroid parent bodies (Halliday et al.

TABLE 1
List of Notations

Variables	Meaning	Definition
M_c	Core mass	
M_e	Embryo mass	See § 2.4
$M_{c,\rm iso}$	Core isolation mass	Eq. (20)
$M_{c,\rm no\ iso}$	Maximum mass of a core	Eq. (22)
$M_{e,\rm iso}$	Embryo isolation mass	Eq. (25)
$M_{e,\rm sca}$	Embryo mass limited by scattering	Eq. (27)
$M_{e,\rm life}$	Embryo mass at $t = \tau_*$ (e.g., 1 Gyr)	Eq. (60)
$M_{c,\rm crit}$	Critical core mass for initiating gas accretion onto the core	Eq. (33)
$M_{c,\rm KH}$	Core mass for Kelvin-Helmholtz contraction time being equal to $\tau_{\rm dep}$	Eq. (31)
M_p	Planet mass including core and envelope	
$M_{g,\rm iso}$	Gas giant isolation mass	Eq. (35)
$M_{g,\rm no\ iso}$	Maximum mass of a gas giant	Eq. (47)
$M_{g,\rm th}$	Gas giant truncation mass by thermal condition	Eq. (38)
$M_{g,\rm vis}$	Gas giant truncation mass by viscous condition	Eq. (37)
$M_{g,\rm feed}$	Supplied gas mass into a feeding zone by viscous diffusion	Eq. (46)
$\tau_{c,\rm acc}$	Core accretion timescale before gas depletion	Eq. (6)
$\tau_{e,\rm acc}$	Embryo accretion timescale after gas depletion	Eq. (9)
$\tau_{\rm dep}$	Depletion timescale of disk gas	Eq. (48)
$\tau_{\rm KH}$	Kelvin-Helmholtz contraction timescale of gas envelope	Eq. (34)
$\tau_{\rm mig}$	Migration timescale of a giant planet	Eq. (65)
Σ_d	Dust surface density of a disk	
Σ_g	Gas surface density of a disk	
$\Sigma_{g,0}$	Initial gas surface density of a disk	Eq. (48)
$\eta_{\rm ice}$	Enhancement factor of Σ_d due to ice condensation	Eq. (11)
f_d	Enhancement factor of Σ_d from a nominal disk	Eq. (11)
f_g	Enhancement factor of Σ_g from a nominal disk	Eq. (12)
$f_{g,0}$	Initial enhancement factor of Σ_g from a nominal disk	Eq. (49)
$f_{\rm disk}$	$= f_{g,0} = f_d$ in this paper	
f_{tg}	Value of $f_{\rm disk}$ to segregate terrestrial/gas giant planet regions	Eq. (50) or eq. (51)
f_{gi}	That to segregate gas/ice giant regions	Eq. (52)
$a_{\rm ice}$	Ice boundary (a semimajor axis of ice condensation)	Eq. (15)
a_{tg}	Semimajor axis to segregate terrestrial/gas giant planet regions	Eq. (53)
a_{gi}	That to segregate gas/ice giant regions	Eq. (54)

2000). Note that even if large-mass cores can be assembled through giant impacts, they can no longer initiate gas accretion because the disk gas needs to be severely depleted prior to their emergence. The limited gas supply during the late phase of core growth through giant impacts is also consistent with the intermediate mass and mostly ice composition of Uranus and Neptune.

In outer regions, the growth of the cores may be terminated before their mass reaches $M_{e,\rm iso}$ or $M_{c,\rm no\ iso}$. When their characteristic surface speed $V_{\rm surf} = (GM_e/R_e)^{1/2}$ exceeds their local escape speed from the host star, $V_{\rm esc} = (2GM_*/a)^{1/2}$, the embryos' 90° grazing scatterings of nearby bodies can lead to the bodies' ejection (Thommes et al. 2003). In this high-σ limit, the ratio of collision to ejection probabilities is $f_{\rm cap} \sim (V_{\rm esc}/V_{\rm surf})^4$. When $f_{\rm cap}$ become significantly less than unity, the growth of the embryos is terminated. Based on previous numerical simulations (Lin & Ida 1997), we set $f_{\rm cap} \sim 0.1$ such that most scatterings lead to ejection and the embryos' asymptotic mass becomes

$$\frac{M_{e,\rm sca}}{R_e} \sim \frac{2 f_{\rm cap}^{-1/2} M_*}{a}, \tag{26}$$

where R_e is the embryos' physical radius. For an average ice embryo, with an internal density $\rho_e \sim 1$ g cm^{-3}, the asymptotic mass of the embryos is

$$M_{e,\rm sca} \sim 2.5 \times 10^2 \left(\frac{\rho_e}{1\ \rm g\ cm^{-3}}\right)^{-1/2} f_{\rm cap}^{-3/4} \left(\frac{a}{1\ \rm AU}\right)^{-3/2} M_\oplus \sim 1.4 \times 10^3 \left(\frac{a}{1\ \rm AU}\right)^{-3/2} M_\oplus. \tag{27}$$

This limiting mass at $a \sim$20–30 AU is comparable to those of the cores of Uranus and Neptune. Note that this limit only applies to the scattering of planetesimals and cores and it is not a limiting mass for gas accretion (see § 3). For notations of masses, timescales, etc., see Table 1.

In principle, the largest cores may emerge with sufficient asymptotic masses to initiate gas accretion (see below). But in many regions, this large mass can only be attained after the gas is depleted. Thus, they are prohibited from evolving into gaseous giant planets. In this paper we consider the formation of the gas giants only if some cores are able to acquire the critical mass for the onset of rapid gas accretion before the disk gas is depleted. We assume that the coalescence between the cores, through giant impacts after the gas depletion, does not lead to substantial further growth in the mass of their gaseous envelopes despite the possibility of substantial increases in their core mass.

2.5. *Core Growth at Different Orbital Radii*

With the above prescriptions, we estimate, with equation (7), the cores' growth rate and asymptotic mass limit. The initial

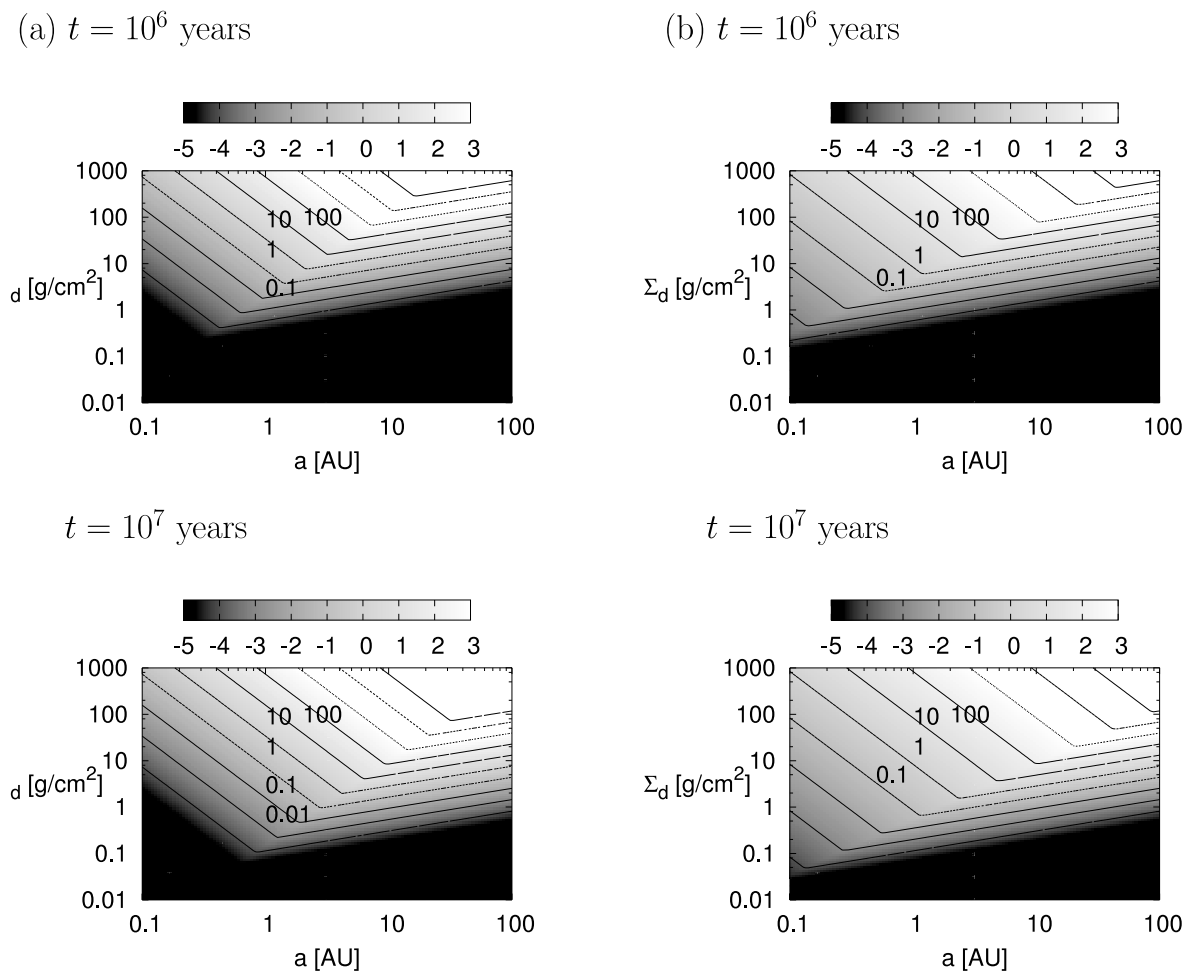

FIG. 3.—(*a*) Analytical estimate of the core mass after 10^6 (*top*) and 10^7 yr (*bottom*). Core mass is truncated by $M_{c,\mathrm{iso}}$. Initial core mass is 10^{20} g. We used $m = 10^{18}$ g, $\Delta a_c = 10 r_{\mathrm{H}}$, and $\Sigma_g/\Sigma_d = 240$. Labels in the contours are $M_c/M_\oplus$. [Numbers of color box are $\log_{10}(M_c/M_\oplus)$.] (*b*) Same as (*a*), except for the truncation by $M_{c,\mathrm{no\ iso}}$ instead of $M_{c,\mathrm{iso}}$. [*See the electronic edition of the Journal for a color version of this figure.*]

mass of the cores is arbitrarily set to be a small value, $M_c = 10^{20}$ g. The choice of an initial value of M_c does not affect the results, since $\tau_{c,\mathrm{acc}}$ increases with M_c. We plot, in Figure 3*a*, the core masses, after 10^6 and 10^7 yr, as a function of Σ_d at various locations a. For this determination, we assume that the growth of the cores is truncated with a mass $M_{c,\mathrm{iso}}$ (eq. [21]). We also assume $\Sigma_g/\Sigma_d = 240$. A similar plot with the cores' truncation mass set by $M_{c,\mathrm{no\ iso}}$ (eq. [22]) instead of $M_{c,\mathrm{iso}}$ is shown in Figure 3*b*.

As shown in equation (7), the cores' growth is relatively fast in regions where Σ_d is high and a is small. The results in Figure 3 show that for this region of the parameter space, the cores' growth is terminated with their asymptotic masses within 10^6 yr. In contrast, the growth is relatively slow for regions of parameter space with relatively small Σ_d and large a so that $M_c(t)$ remains very low in the bottom right regions in Figure 3. An "accretion wave" propagates from the top left to the bottom right regions as time passes. In the very large Σ_d and large-a regions, $\Delta a_c \sim 10 r_{\mathrm{H}}$ for $M_{c,\mathrm{iso}}$ exceeds the magnitude of a. Thus, the appropriate expression for the truncation mass is $M_{c,\mathrm{no\ iso}}$ rather than $M_{c,\mathrm{iso}}$ in these regions.

Next, we consider planetary systems with a Σ_d distribution similar to that derived from a minimum-mass solar nebula model (see eq. [11]). Figure 4 shows some examples of the time evolution of the cores' masses for $f_d = 1$ (Fig. 4*a*) and $f_d = 10$ (Fig. 4*b*). The jumps in the cores' masses at 2.7 AU in these figures reflect a transition in the values of Σ_d. These results indicate that in the inner regions of the disk, the gas depletion timescale is longer than the buildup timescale for the cores and all the field planetesimals are accreted onto the isolated cores. However, for the minimum-mass solar nebula model (with $f_d \simeq 1$), $M_{c,\mathrm{iso}}$ at 0.7 and 1 AU is considerably smaller than the present masses of Venus and Earth (see eq. [21]). These planets could have acquired their present mass through either giant impacts after depletion of the gas or the accretion of planetesimals prior to the gas depletion if they have diffused or migrated over large radial distances. In this case, the cores' asymptotic mass would be $M_{e,\mathrm{iso}}$ (eq. [25]) or $M_{c,\mathrm{no\ iso}}$ (eq. [23]), which, at 0.7 and 1 AU, is comparable to the mass of the Earth and Venus.

For a more comprehensive parameter study, we show in Figure 5 the dependence of the cores' mass on a and f_d after 10^6 and 10^7 yr. In these calculations, f_g does not decline and is set to

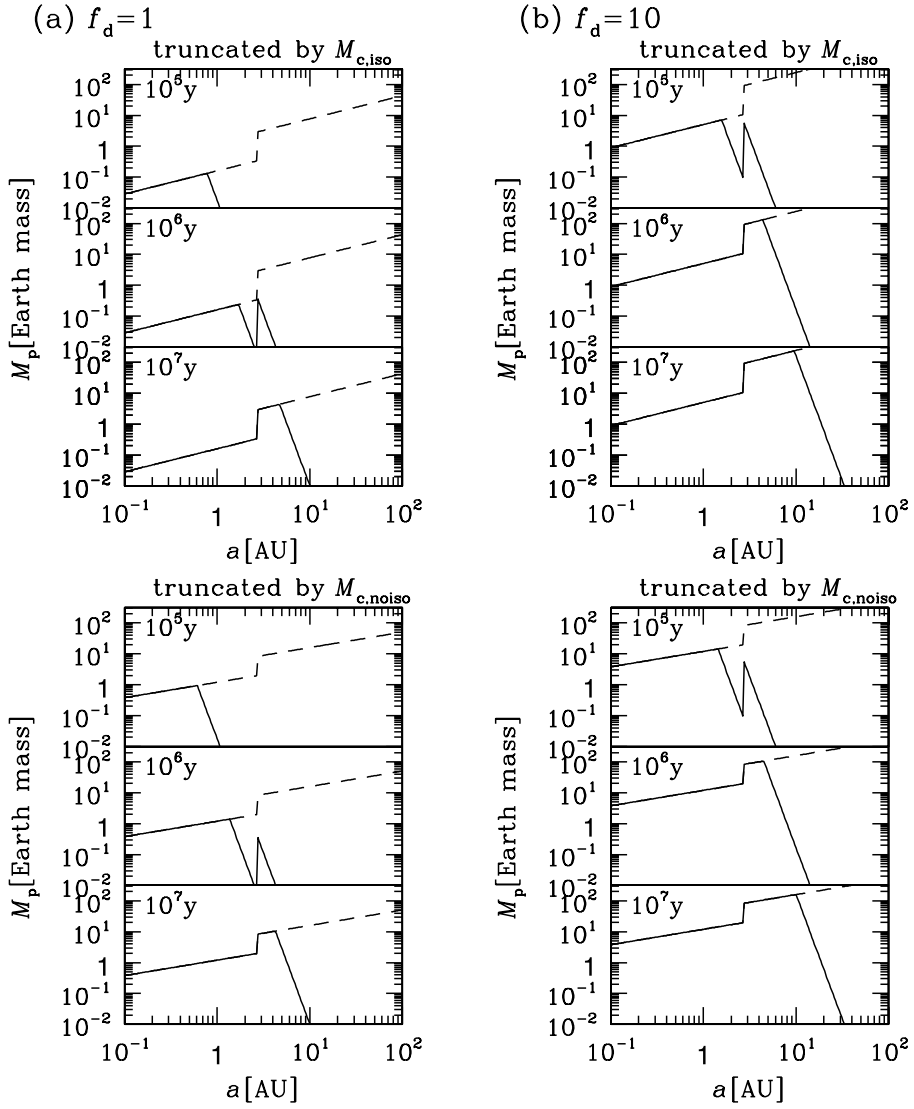

FIG. 4.—Time evolution of core mass (10^5, 10^6, and 10^7 yr), shown by sold lines, in the case of (*a*) $f_d = 1$ and (*b*) $f_d = 10$. Core mass is truncated by $M_{c,\mathrm{iso}}$ (*top panels*) or by $M_{c,\mathrm{no\ iso}}$ (*bottom panels*), which are shown by the dashed lines. The jumps at 2.7 AU are caused by increase in solid materials due to ice condensation.

be always equal to f_d since the stages prior to depletion of the gas are considered. The magnitude of Σ_d for the minimum-mass solar nebula model corresponds to $f_d \simeq 1$. On the gas depletion timescale $\sim 10^6$–10^7 yr, the most massive cores attain a critical mass (approximately several $M_\oplus$) just outside the ice boundary (2.7 AU). Although the magnitude of both $M_{c,\mathrm{no\ iso}}$ and $M_{c,\mathrm{iso}}$ increases with a, the expression in equation (17) indicates that much beyond a_{ice}, the cores do not have sufficient time to attain their asymptotic values prior to the depletion of the disk gas. In this case, the formation of gas giants within a minimum-mass solar nebula is most likely to be initiated just outside the ice boundary. But around many classical T Tauri stars, the disk mass inferred from the millimeter-wave length continuum observation corresponds to $f_d \gtrsim 5$ (see § 1). The results in Figures 5*a* and 5*b* suggest that in very massive protoplanetary disks with $f_d \gtrsim 5$, cores can rapidly attain masses greater than the critical mass for gas accretion (see next section) even inside the ice boundary.

After the gas depletion, $M_{c,\mathrm{iso}}$ expands to $M_{c,\mathrm{no\ iso}}$ or $M_{e,\mathrm{iso}}$. $M_{e,\mathrm{sca}}$ can also limit embryo growth (see § 4.2.3 and Fig. 10). In the calculations in the following sections, we set the asymptotic masses of cores and embryos as follows:

1. The isolated core model: min $(M_{c,\mathrm{iso}}, M_{c,\mathrm{no\ iso}})$, when $f_g > 10^{-3}$ (before the gas depletion); min $(M_{e,\mathrm{iso}}, M_{c,\mathrm{no\ iso}}, M_{e,\mathrm{sca}})$, when $f_g < 10^{-3}$ (after the gas depletion).
2. The nonisolated core model: $M_{c,\mathrm{no\ iso}}$, when $f_g > 10^{-3}$; min $(M_{c,\mathrm{no\ iso}}, M_{e,\mathrm{sca}})$, when $f_g < 10^{-3}$.

3. GAS ACCRETION

Up to now, we only consider the drag effect induced by the gas on the damping of the planetesimals' and cores' velocity dispersion. In this section we consider the accretion of gas onto sufficiently massive cores. The necessary condition for any gas accumulation near the cores is that their surface escape velocity must exceed the sound speed of the disk gas. In regions of the

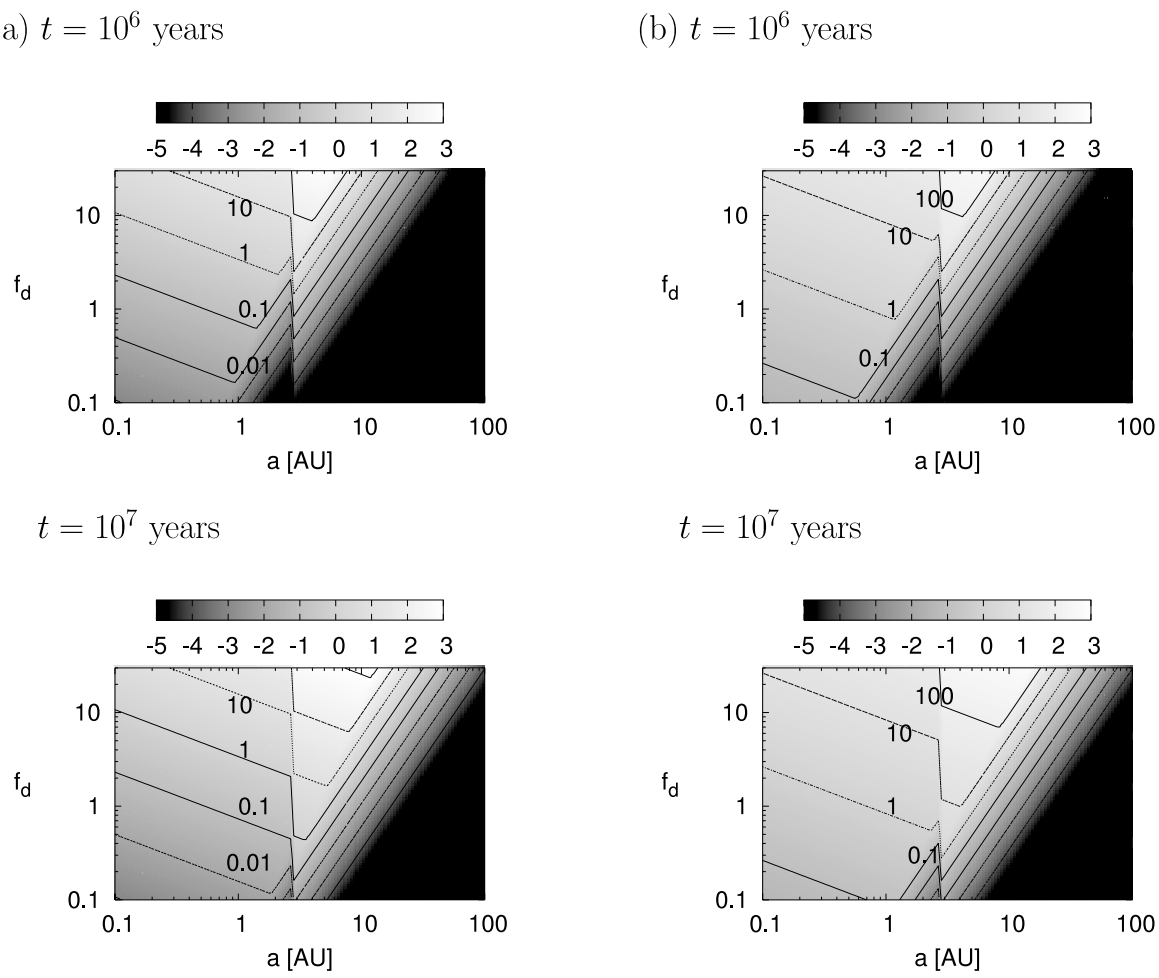

FIG. 5.—Core masses after 10^6 (*top*) and 10^7 yr (*bottom*) as a function of a and f_d. (*a*) Core mass is truncated by $M_{c,\mathrm{iso}}$. (*b*) Truncation by $M_{c,\mathrm{no\,iso}}$. [*See the electronic edition of the Journal for a color version of this figure.*]

disk where dust can condense to form planets, the sound speed is less than a few kilometers per second such that even lunar-mass cores can attract gas to their proximity. However, the disk gas first accumulates into a static envelope around these cores. In this envelope, the gravity of the cores is balanced by a pressure gradient that is maintained by the energy release during the planetesimals' bombardment onto the cores.

3.1. *Gas Accretion onto Cores*

However, when the cores' mass (M_c) becomes larger than a critical value ($M_{c,\mathrm{crit}}$), the state of quasi-hydrostatic equilibrium can no longer be maintained and a phase of gas accretion onto the core is initiated (Mizuno 1980; Bodenheimer & Pollack 1986). Thereafter, the planetesimals and gas accretion proceed concurrently, so that the planetary growth can no longer be expressed in an analytical form as that in equation (17). Based on the existing numerical results, we adopt a simple prescription to evaluate $M_{c,\mathrm{crit}}$ and the gas accretion rate, $dM_{p,g}/dt$.

The critical core mass depends on the cores' rate of planetesimal accretion ($\dot{M}_c$) and the opacity (κ) associated with the disk gas. Faster accretion and higher opacity (relatively large $\dot{M}_c$ and κ) result in a warmer planetary atmosphere and the enhanced pressure gradient stalls the gas accretion (Stevenson 1982; Ikoma et al. 2000). The value of $M_{c,\mathrm{crit}}$ is regulated by the inefficient radiative layers in the envelope. Instabilities may be induced by rotation and molecular weight gradient in the radiative layers such that the magnitude of $M_{c,\mathrm{crit}}$ may also be reduced and the production of gas giants may be more prolific.

In the absence of any quantitative multidimensional models, we adopt the results obtained from spherically symmetric thoroughly mixed models. Based on a series of numerical models, Ikoma et al. (2000) find that the critical core mass has the following dependence:

$$M_{c,\mathrm{crit}} \simeq 10\left(\frac{\dot{M}_c}{10^{-6}\ M_\oplus\ \mathrm{yr}^{-1}}\right)^{0.2-0.3}\left(\frac{\kappa}{1\ \mathrm{cm}^2\ \mathrm{g}^{-1}}\right)^{0.2-0.3} M_\oplus. \tag{28}$$

We adopt here a power-law index $\frac{1}{4}$ for the dependence on $\dot{M}_c$. If the dust particles have a similar distribution and abundance as the interstellar medium, $\kappa \sim 1\ \mathrm{cm}^2\ \mathrm{g}^{-1}$. The actual magnitude of κ is uncertain since the dust particles' size distribution and the fraction of heavy element in the gas and solid phases are poorly known (Podolak 2003). For computational simplicity, we neglect the dependence of $M_{c,\mathrm{crit}}$ on κ in our prescription below.

The gaseous envelope of proto–giant planets contracts on a Kelvin-Helmholtz timescale when their masses M_p (including both their solid cores and gaseous envelope) become larger than $M_{c,\rm crit}$. Ikoma et al. (2000) derived through numerical calculation that

$$\tau_{\rm KH} \simeq 10^b \left(\frac{M_p}{M_\oplus}\right)^{-c} \left(\frac{\kappa}{1\ {\rm g\ cm^{-2}}}\right)\ {\rm yr}, \tag{29}$$

with power-law index $b \simeq 8$ and $c \simeq 2.5$. However, with a different opacity table, the values of b and c can be changed to $\simeq$10 and $\simeq$3.5, respectively (M. Ikoma 2003, private communication). Bryden, Lin, & Ida (2000a) obtained $b \simeq 10$, $c \simeq 3.0$ by fitting the result of Pollack et al. (1996). We adopt here $b = 9$ and $c = 3.0$ and also neglect the dependence on κ in our prescription below.

The contraction of the gas envelope reduces the local pressure gradient. Consequently, the gas from the surrounding disk flows toward the cores to replenish the envelope at a rate

$$\frac{dM_{p,g}}{dt} \simeq \frac{M_p}{\tau_{\rm KH}}. \tag{30}$$

This rate is well below the Bondi accretion rate (Bondi 1952) when $M_p \sim M_{c,\rm crit}$, so the gas accretion rate is insensitive to the boundary condition in the disk. The magnitude of $dM_{p,g}/dt$ due to the Kelvin-Helmholtz contraction increases rapidly with M_p. In principle, $dM_{p,g}/dt$ is limited by the Bondi accretion rate (Bondi 1952), the Keplerian shear in the gas inflow (Tanigawa & Watanabe 2002), the mass diffusion rate through the disk (Bryden et al. 1999), and the availability of gas near the orbit of the accreting planet. However, these effects become important only when M_p has already become a significant fraction of Jupiter's mass $M_{\rm J}$. For $M_p \sim M_{\rm J}$, $\tau_{\rm KH}$ is reduced to the dynamical free-fall timescale and the growth timescale $M_p/(dM_{p,g}/dt)$ for Bondi accretion is reduced to 10^3 yr. Thus, the total gas accretion time for the protoplanets to attain their asymptotic masses is essentially determined by $\tau_{\rm KH}$ at $M_p \sim M_{c,\rm crit}$.

Note that when M_c reaches $M_{c,\rm iso}$, $\dot{M}_c$ is reduced to zero. Consequently, $M_{c,\rm crit}$ also vanishes and gas accretion can start for any value of M_c. However, if

$$M_c \lesssim M_{c,\rm KH} \equiv M_p(\tau_{\rm KH} = \tau_{\rm disk}) \simeq 4.6 \left(\frac{\tau_{\rm disk}}{10^7\ {\rm yr}}\right)^{-1/3} M_\oplus, \tag{31}$$

the gas accretion rate is so small (eq. [30]) that M_p is not significantly increased by the gas accretion during the first 10^7 yr after they were formed. In order for the gas giants to actually form and acquire $M_p \gg M_{c,\rm crit}$, M_c must be larger than $M_{c,\rm KH}$ in addition to the requirement of $M_c > M_{c,\rm crit}$. Both conditions can be satisfied for $M_c \gtrsim 4\ M_\oplus$, if the cores' rate of planetesimal accretion is significantly reduced from that in equation (3).

3.2. *A Prescription for the Growth of Gas Giant Planets*

Based on the above considerations, we introduce the following simple prescription for the purpose of numerically integrating the formation and early evolution of the gaseous giant planets. This approximation captures the essence of the planet formation process.

1. Protoplanetary growth due to planetesimal accretion is computed with the following rate equation:

$$\frac{dM_{p,\rm pl}}{dt} = \frac{M_p}{\tau_{c,\rm acc}} = \dot{M}_c\left(M_c = M_p\right), \tag{32}$$

where $\tau_{c,\rm acc}$ is given by equation (18). The value of $\dot{M}_c$ is obtained from equation (3) with the core mass M_c being replaced by the protoplanet's total mass M_p, which also includes the mass of the gaseous envelope.

2. During the growth of the cores, we check whether M_p is less than the critical core mass for the onset of gas accretion. Based on the discussions in the previous subsection, the magnitude of $M_{c,\rm crit}$ is approximated with a simplified version of equation (28) such that

$$M_{c,\rm crit} \simeq 10 \left[\frac{\dot{M}_c\left(M_c = M_p\right)}{10^{-6}\ M_\oplus\ {\rm yr^{-1}}}\right]^{1/4} M_\oplus. \tag{33}$$

In principle, as the field planetesimals are being accreted onto the cores, their surface density in the feeding zone declines, so that both $\dot{M}_c$ and $M_{c,\rm crit}$ decrease. To take this effect into account, we use time-dependent values of $\dot{M}_c$ calculated in equation (32) and set $M_{c,\rm crit} = 0$ for cores with $M_c > M_{c,\rm iso}$ or $M_{c,\rm no\ iso}$.

3. When M_c exceeds $M_{c,\rm crit}$, gas accretion onto a core is set to start. The gas accretion rate is regulated by the efficiency of heat transfer and is approximated by a simplified version of equations (29) and (30) such that

$$\frac{dM_{p,g}}{dt} \simeq \frac{M_p}{\tau_{\rm KH}},$$
$$\tau_{\rm KH} \simeq 10^9 \left(\frac{M_p}{M_\oplus}\right)^{-3}\ {\rm yr}. \tag{34}$$

The planets' mass M_p includes both their gaseous envelope and cores. Because of the expansion of the growing planets' feed zones, planetesimal accretion onto the cores continues after the gas accretion has started. However, we neglect the collisions between cores until after the disk gas is depleted as we have discussed in the last section.

4. The above gas accretion rate does not explicitly depend on the ambient conditions. The approximation is appropriate provided that there is an adequate supply of the disk gas. However, the disk gas may be depleted either globally through processes such as the viscous evolution, outflow, and photoevaporation or locally through gap formation. These effects are taken into account in the determination of the asymptotic mass of the giant planets (see the next subsection) but not in their accretion rates.

5. In the limit that the growth of the gas giant planets is terminated by gap formation, we also consider their dynamical evolution with or without the type II orbital migration (see the next section).

3.3. *Termination of Gas Accretion*

Equation (34) shows that the gas accretion rate rapidly increases with M_p. However, there are several asymptotic limits to the unimpeded runaway gas accretion process. These limits arise as a result of the local and global depletion of disk gas.

3.3.1. *Local Gas Depletion*

In an inviscid disk, gas accretion onto the cores is terminated when they consume all the gas in their feeding zone and attain an isolation mass. The isolation mass for the gas giants can be obtained by replacing Σ_d in equation (20) with Σ_g such as

$$M_{g,\rm iso} \simeq 50\left(\frac{\Sigma_g}{2.4\times10^3\ {\rm g\ cm^{-2}}}\right)^{3/2}\left(\frac{a}{1\ {\rm AU}}\right)^3 \times\left(\frac{\Delta a_g}{2r_{\rm H}}\right)^{3/2}\left(\frac{M_*}{M_\odot}\right)^{-1/2} M_\oplus, \quad (35)$$

where the Hill (Roche lobe) radius $r_{\rm H}$ is evaluated with M_p. For a fiducial magnitude of $M_{g,\rm iso}$, we used the width of gas feeding zone $\Delta a_g = 2r_{\rm H}$ to be a nominal value. Since it flows normally on circular orbits, gas that is much beyond Δa_g cannot reach the accreting cores without modifying their specific angular momentum. Using the Σ_g distribution in equation (12), we find

$$M_{g,\rm iso} \simeq 50 f_g^{3/2}\left(\frac{a}{1\ {\rm AU}}\right)^{3/4}\left(\frac{\Delta a_g}{2r_{\rm H}}\right)^{3/2}\left(\frac{M_*}{M_\odot}\right)^{-1/2} M_\oplus, \quad (36)$$

which is comparable to $M_{\rm J}$ at the present location of Jupiter. Since Σ_g and equivalently f_g decrease with time, $M_{g,\rm iso}$ also decreases with time. The $dM_{p,g}/dt$ is set to be zero when M_p becomes larger than $M_{g,\rm iso}$.

However, the observed accretion flow from protostellar disks to their host stars (Hartmann et al. 1998) requires mass and angular momentum transfer throughout the disks. In a viscously evolving disk, gas can continuously diffuse into the feeding zone until the growing planet attains a mass (Lin & Papaloizou 1985)

$$M_{g,\rm vis} \simeq \frac{40\nu}{a\Omega_{\rm K}} M_* \simeq 40\alpha\left(\frac{h}{a}\right)^2 M_* \simeq 30\left(\frac{\alpha}{10^{-3}}\right)\left(\frac{a}{1\ {\rm AU}}\right)^{1/2}\left(\frac{M_*}{M_\odot}\right) M_\oplus, \quad (37)$$

where we used equation (16) and α-prescription for the effective viscosity ν (Shakura & Sunyaev 1973), in which $\nu = \alpha h^2\Omega_{\rm K}$, where α is a dimensionless parameter. For $M_p > M_{g,\rm vis}$, an embedded planet induces a strong tidal torque to open a gap near its orbit, provided that its Hill (Roche lobe) radius is larger than a critical value $r_{{\rm H},c} = h$ (Lin & Papaloizou 1993; Bryden et al. 2000b). We find that $r_{\rm H} = r_{{\rm H},c}$ when

$$M_{g,\rm th} \simeq 3.8\times10^{-4}\left(\frac{a}{1\ {\rm AU}}\right)^{3/4} M_* \simeq 1.2\times10^2\left(\frac{a}{1\ {\rm AU}}\right)^{3/4}\left(\frac{M_*}{M_\odot}\right) M_\oplus. \quad (38)$$

Because $M_{g,\rm th}$ is generally larger than $M_{g,\rm vis}$ except for some very large α cases, gas inflow onto the planet would actually be halted, when M_p reaches $M_{g,\rm th}$. In some previous hydrodynamic simulations, embedded protoplanets continue to accrete after the above condition is satisfied albeit at a reduced rate (Artymowicz & Lubow 1996). In order to take this possibility into account, we also modify, in one set of calculations, the truncation condition to $r_{{\rm H},c} = 1.5h$.

3.3.2. *Global Gas Depletion*

Before their M_p increases to the isolation mass, $M_{\rm gas,iso}$, protoplanets can accrete at the rate given in equation (34). However, for $M_p > M_{\rm gas,iso}$, additional disk material can no longer be brought into the feeding zone by the expansion of its boundary. Nevertheless, in a viscously evolving disk, the feeding zone may be replenished. We also consider the extreme case that the protoplanets' tidal interaction does not impinge the flow of the gas from the disk to their feeding zone.

Although gas diffusion can replenish the feeding zone, the rate of gas accretion onto the protoplanet is limited to

$$\frac{dM_{p,g}}{dt} = \min\left(\frac{M_p}{\tau_{\rm KH}}, \dot{M}_{\rm disk}\right), \quad (39)$$

where the mass transfer rate in the disk

$$\dot{M}_{\rm disk} = 2\pi\Sigma_g a V_{\rm disk}. \quad (40)$$

The gas diffusion speed is determined by the efficiency of viscous transport

$$V_{\rm disk} \simeq -\frac{3\nu}{a}\left[\frac{\partial\ln\left(\Sigma_g\nu\right)}{\partial\ln a}+\frac{1}{2}\right]. \quad (41)$$

With the α-prescription for a steady disk, $V_{\rm disk} \sim -\alpha h^2\Omega_{\rm K}/a$.

The magnitude of α in the planet formation region is uncertain. We assume that the mass transfer rate throughout the disk is comparable to an observational inferred accretion rate from protostellar disks onto classical T Tauri stars (Hartmann et al. 1998), which can be fitted by

$$\dot{M}_{\rm disk} \sim \dot{M}_0\left(\frac{t}{\tau_{\rm disk}}\right)^{-1.5}, \quad (42)$$

where $\dot{M}_0 = 10^{-4}\,M_\oplus\,{\rm yr}^{-1}$ for $\tau_{\rm disk} = 10^7$ yr (Calvet, Hartmann, & Strom 2000). The actual data have an order-of-magnitude spread over this fit. The accretion rate onto the planets is limited by the gas replenishment rate of their feeding zone, $\dot{M}_{\rm disk}$, when their

$$\frac{M_p}{\tau_{\rm KH}} > \dot{M}_{\rm disk}, \quad (43)$$

or equivalently when their M_p becomes larger than

$$M_{g,\rm sup}(t) \simeq 20\left(\frac{t}{10^7\ {\rm yr}}\right)^{-3/8} M_\oplus \quad (44)$$

(see eqs. [29] and [43]). The limiting replenishment rate only modifies $dM_{p,\rm gas}/dt$ for protoplanets more massive than both $M_{g,\rm sup}$ and $M_{g,\rm iso}$. From equations (36) and (49), we find that these conditions are satisfied at the advanced stages of disk evolution when the surface density of the disk is significantly depleted.

At any given location, the emergence of cores that can dynamically accrete gas occurs at an epoch

$$\tau_{\rm onset} = 3\tau_{c,\rm acc}\left(M_c = M_{c,\rm crit}\right) \sim 8\times10^5\eta_{\rm ice}^{-1}f_d^{-7/5}\left(\frac{a}{1\ {\rm AU}}\right)^{27/10}\left(\frac{M_{c,\rm crit}}{10\ M_\oplus}\right)^{1/3}\ {\rm yr} \quad (45)$$

for $M_* = 1\ M_\odot$. According to equation (42), the amount of mass that can be supplied into the feeding zone for $t > \tau_{\rm onset}$ is

$$M_{g,\rm feed} = \int_{\tau_{\rm onset}}^{\infty} \dot{M}_{\rm disk}(t)\, dt \simeq 1.5 \dot{M}_{\rm disk}(t = \tau_{\rm onset})\tau_{\rm disk} \simeq 60 \left(\frac{\eta_{\rm ice}}{4}\right)^{3/2} f_d^{21/10} \left(\frac{a}{10\ {\rm AU}}\right)^{-81/20} \left(\frac{\tau_{\rm disk}}{10^7\ {\rm yr}}\right)^{5/2} M_\oplus. \quad (46)$$

If such a supply is considered, the isolation mass can increase from $M_{g,\rm iso}$ to $M_{g,\rm iso} + M_{g,\rm feed}$. However, at large a, $M_{g,\rm feed}$ is not large enough. Since sufficiently massive cores (with $M_c > M_{c,\rm crit}$) take longer to form in the outer regions of the disk, the mass transfer rate can limit the amount of material supplied to the feeding zone, $M_{g,\rm feed}$, to less than the mass of Jupiter.

The gas accretion is ultimately limited by the amount of residual gas in the entire disk. For our disk model, the maximum available mass is

$$M_{g,\rm no\ iso} \sim \pi a^2 \Sigma_g \simeq 290 \left(\frac{\Sigma_g}{2.4 \times 10^3\ {\rm g\ cm^{-2}}}\right)\left(\frac{a}{1\ {\rm AU}}\right)^2 M_\oplus \simeq 290 f_g \left(\frac{a}{1\ {\rm AU}}\right)^{1/2} M_\oplus. \quad (47)$$

When $M_{g,\rm no\ iso} < M_{g,\rm th}$, M_p is truncated by $M_{g,\rm no\ iso}$ rather than $M_{g,\rm th}$. This condition occurs when $f_g < 3(a/1\ {\rm AU})^{1/4} (M_*/M_\oplus)^{5/2}$. Similar to $M_{g,\rm iso}$, $M_{g,\rm no\ iso}$ explicitly depends on the magnitude of f_g, i.e., the amount of residual gas in the disk.

As we have already indicated in § 2, the gas content is observed to decline concurrently with the dust (but not the planetesimal) content in protostellar disks. Since the near-IR signature for dust in the inner region declines together with the millimeter indicators of dust in the outer regions of protostellar disks (Duvert et al. 2000), we assume that the residual gas in the these disks is depleted globally in a self-similar manner. We introduce a prescription to approximate the evolution of Σ_g during the depletion phase of the disk such that

$$\Sigma_g \simeq \Sigma_{g,0} \exp\left(-\frac{t}{\tau_{\rm disk}}\right), \quad (48)$$

where $\Sigma_{g,0}$ is an initial distribution (eq. [12]) and $\tau_{\rm disk}$ is the gas depletion timescale. Equivalently, f_g decreases with time from its initial value $f_{g,0}$ as

$$f_g \simeq f_{g,0} \exp\left(-\frac{t}{\tau_{\rm disk}}\right). \quad (49)$$

Based on the observed properties of protostellar disks (Beckwith & Sargent 1996; Wyatt et al. 2003), we set $\tau_{\rm disk} = 10^7$ yr.

In order to limit the extent of the parameter studies, we also assume here that $f_{g,0} = f_d$, that is, the gas-to-dust ratio is initially equal to the solar composition. We denote both $f_{g,0}$ and f_d to be $f_{\rm disk}$. We consider the cases with $f_{\rm disk} = 0.1$–30 as mentioned in the last section. We do not vary the value of $f_{\rm disk}$ during the cores' growth, but it is locally set to zero when the cores have reached their asymptotic masses.

Based on these prescriptions, we set an asymptotic mass for the gas giants. We assume that the gas accretion onto it is terminated when a proto–giant planet either consumes all the nearby residual gas in the disk or has acquired a sufficiently large mass to open up a gap near its orbit.

4. NASCENT ORBITAL DISTRIBUTION OF PROTOPLANETS

In this section we consider dynamical properties such as the mass and semimajor axis distributions with which planets are formed. This distribution evolves with the orbital migration of the gas giant planets. We discuss the effect of orbital migration in the next section.

4.1. *Conditions for the Emergence of Gaseous and Ice Giant Planets*

We compute a series of models with $\tau_{\rm disk} = 10^7$ yr. We determine the asymptotic (at $t = 10^9$ yr) magnitude of M_p, including that of the gaseous envelope if any, as a function of $f_{\rm disk}$ ($= f_d = f_{g,0}$) and a (see Fig. 6). For these models, we adopt isolated cores (§ 2.5), and five different prescriptions for the planets' asymptotic mass after their gas accretion is truncated: $M_{g,\rm iso}$ (Fig. 6*a*), $M_{g,\rm no\ iso}$ (Fig. 6*b*), $M_{\rm gas,vis}$ (Fig. 6*c*), $M_{g,\rm th}$ (Fig. 6*d*), and $M_{g,\rm iso} + M_{g,\rm feed}$ (Fig. 6*e*). For the evaluation of the asymptotic mass of the gas giants, we adopt $\Delta a_g = 2r_{\rm H}$ in Figures 6*a* and 6*e*, $M_* = 1\ M_\odot$ in Figures 6*c* and 6*d*, and $\alpha = 10^{-3}$ in Figure 6*c*. Since the result of Figure 6*e* is almost the same as that of Figure 6*d*, it is omitted. There are some uncertainties in the amount of gas diffusion to the planet's feeding zone. These five upper mass limits provide a range in the asymptotic mass of the planets. In Figure 7 we show the results of a second series of models computed with the non-isolated core model (§ 2.5). All other parameters are identical to the first series of models.

For disks with a uniform $f_{\rm disk} \sim 1$–3, there are three distinct regions in Figure 6. Similar regions also exist in Figure 7 for a disk with uniform $f_{\rm disk} \sim 0.3$–1. In the inner ($a < a_{\rm ice}$) regions, the asymptotic mass of the cores M_c is smaller than 4 $M_\oplus$, which is the minimum mass ($M_{c,\rm KH}$) needed to undergo a significant amount of gas accretion within 10^7 yr. Since gas is depleted on this timescale, gas giants cannot form in these regions. Although after gas depletion the cores' mass can exceed several $M_\oplus$ through giant impacts between them, they can no longer accrete gas. These massive cores evolve into terrestrial planets similar to the Earth, and the mass distinction between the terrestrial planets and gas giants is preserved.

In the outer regions of the disk where $a \gtrsim 10$–20 AU, the cores' planetesimal accretion rate is very low. Although the asymptotic mass limit for the cores is large compared with several $M_\oplus$, there is an inadequate amount of time for the cores to attain a significant amount of mass prior to the depletion of the disk gas. Nevertheless, low-mass cores can slowly accrete gas because, for very low planetesimal accretion rates $\dot{M}_c$, the values of $M_{c,\rm crit}$ are also small. However, in the low-$\dot{M}_c$ limit, the gas disk is severely depleted by the time M_c becomes comparable to $M_{c,\rm KH}$. In advanced stages of gas depletion, the magnitude of both $M_{g,\rm iso}$ and $M_{g,\rm no\ iso}$ becomes smaller than M_c and the cores cannot acquire a massive gaseous envelope. This limited supply of residual disk gas may have quenched the ability of Uranus and Neptune to attain a massive envelope ($\lesssim 2\ M_\oplus$) despite their present ice core mass being $\gtrsim 15\ M_\oplus$ (Pollack et al. 1996). We refer to these heavy-element–enhanced latecomers with modest gaseous envelopes as ice giant planets.

In the intermediate region slightly outside the ice boundaries, an abrupt increase in the cores' asymptotic mass allows the cores to initiate the onset of rapid gas accretion. Gas giants with $M_p \gtrsim 100\ M_\oplus$ are preferentially formed in this bright

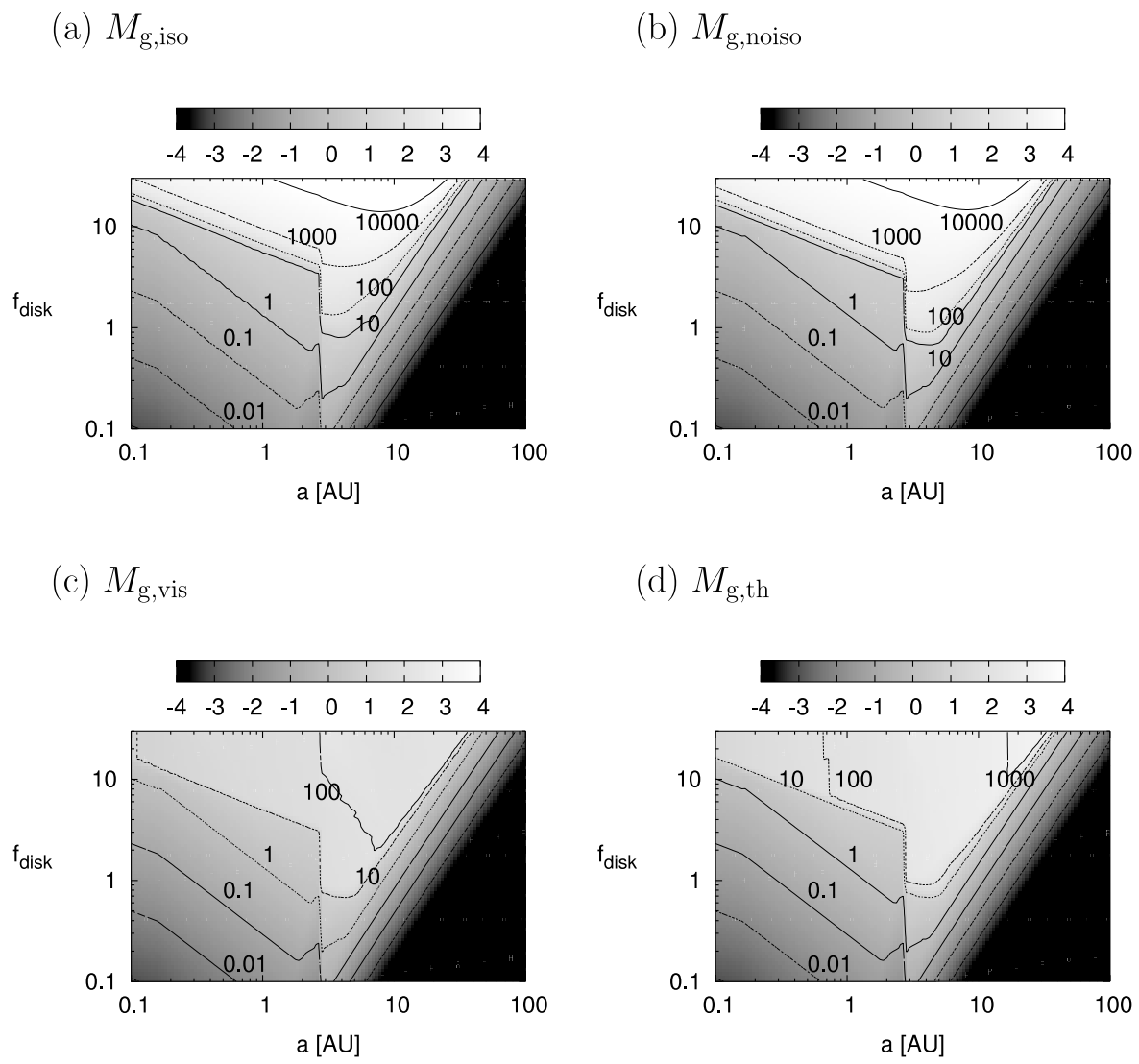

FIG. 6.—Planet masses including gas envelope at 10^9 yr as a function of $f_{\rm disk}$ ($=f_d=f_{g,0}$) and a. Here $\tau_{\rm disk}=10^7$ yr and $a_{\rm ice}=2.7$ AU are adopted. Cores are truncated by $M_{c,\rm iso}$ (after f_g declines below 10^{-3}, truncated by $M_{e,\rm iso}$). Gas accretion is truncated at (*a*) $M_{g,\rm iso}$, (*b*) $M_{g,\rm no\ iso}$, (*c*) $M_{g,\rm vis}$, and (*d*) $M_{g,\rm th}$. We adopt $\Delta a_g=2r_{\rm H}$ in (*a*), $M_*=1\ M_\odot$ in (*c*) and (*d*), and $\alpha=10^{-3}$ in (*c*). Labels in the contours are $M_p/M_\oplus$. [Numbers of color box are $\log_{10}(M_p/M_\oplus)$.] [*See the electronic edition of the Journal for a color version of this figure.*]

region in Figures 6 and 7. The boundaries of the region where gas giants can form are set by the requirements that (1) $M_c \gtrsim 4\ M_\oplus$ and (2) $3\tau_{c,\rm acc} \lesssim \tau_{\rm disk}$. The results in Figures 6 and 7 indicate that conditions 1 and 2 are satisfied, for $f_{\rm disk} \gtrsim 1$, at $a_{tg} \gtrsim 3$ AU (the "rocky/gas giant planets' boundary") and $a_{gi} \lesssim 10$–20 AU (the "gas/ice giants' boundary"). Terrestrial planets form inside a_{tg}, and ice giants form outside a_{gi}. The values of a_{tg} and a_{gi} are expressed in equations (53) and (54).

We now consider a_{tg} and a_{gi} for more general values of $f_{\rm disk}$. Transition from cores to gas giants requires gas accretion and can only occur prior to gas depletion. However, in the presence of gas, the core growth is limited by their asymptotic masses. If the asymptotic mass is determined by the isolation process, it would become $M_{c,\rm iso}$. In this case, condition 1 can only be satisfied if $M_{c,\rm iso} > 4\ M_\oplus$. From equation (21), this necessary condition corresponds to

$$f_{\rm disk} \gtrsim f_{tg} \simeq 8\eta_{\rm ice}^{-1}\left(\frac{a}{1\ \rm AU}\right)^{-1/2}. \tag{50}$$

Similarly, in the nonisolated limit, the condition that $M_{c,\rm no\ iso} > 4\ M_\oplus$ corresponds to

$$f_{\rm disk} \gtrsim f_{tg} \simeq 3\eta_{\rm ice}^{-1}\left(\frac{a}{1\ \rm AU}\right)^{-1/2} \tag{51}$$

(see eq. [23]). These estimates agree with the terrestrial/gas giant planets' boundary in Figures 6 and 7, respectively. In comparison with the results in the first series, the emergence of the more massive cores in the second series of simulations enhances the probability and speeds up the onset of gas giant formation for modest values of a.

In condition 2 ($3\tau_{c,\rm acc} \lesssim \tau_{\rm disk}$), the quantity $3\tau_{c,\rm acc}$ is the actual growth timescale for the cores (see eq. [18]). From

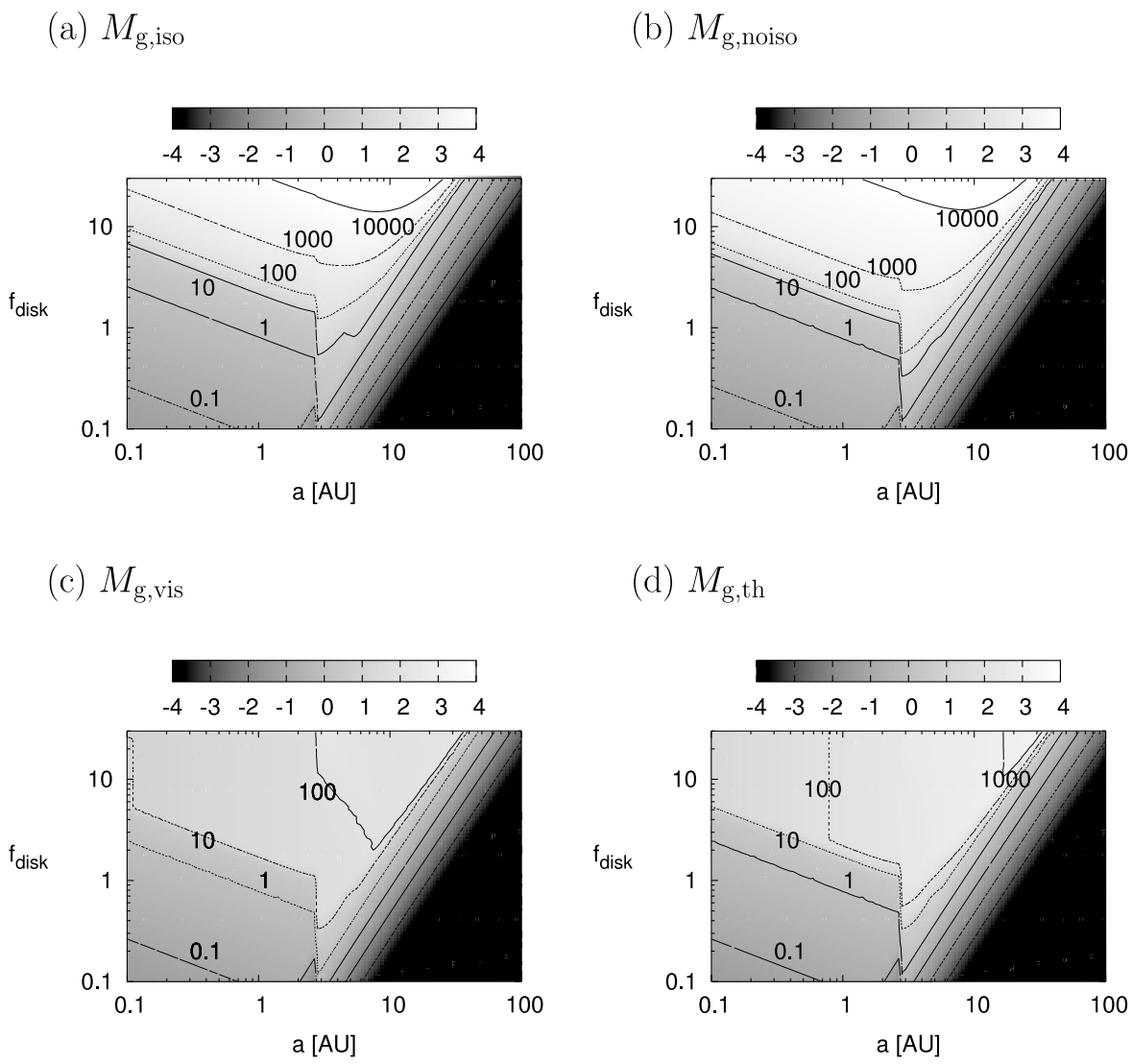

FIG. 7.—Same as Fig. 6, butt for core truncation by $M_{c,\rm no\ iso}$. [*See the electronic edition of the Journal for a color version of this figure.*]

equation (18), the condition for $3\tau_{c,\rm acc} \simeq \tau_{\rm disk}$ corresponds to

$$f_{\rm disk} \gtrsim f_{gi} \simeq 4\left(\frac{\eta_{\rm ice}}{4}\right)^{-5/7}\left(\frac{M_p}{4\ M_\oplus}\right)^{5/21} \times \left(\frac{\tau_{\rm dep}}{10^7\ {\rm yr}}\right)^{5/7}\left(\frac{a}{10\ {\rm AU}}\right)^{27/14}. \quad (52)$$

This condition does not depend on whether the asymptotic mass of the cores is limited by $M_{c,\rm iso}$ or $M_{c,\rm no\ iso}$. For $\eta_{\rm ice} = 4$, $M_p = 4\ M_\oplus$, and $\tau_{\rm disk} = 10^7$ yr, this equation indicates that $f_{gi} \simeq 4(a/10\ {\rm AU})^{1/2}$, which also agrees well with the gas/ice giants' boundary in Figures 6 and 7.

As the analytical derivation shows, the two boundaries separating the three regions nurture the formation of terrestrial planets, gas giants, and ice giants and do not depend on conditions of truncation of gas accretion. In the outer regions of the disk, the gas/ice giants' boundary is also insensitive to the asymptotic mass of the cores. At large a, the barrier for reaching $M_{c,\rm crit}$ is imposed by the persistence of disk gas on timescales $\tau_{\rm disk}$ rather than the asymptotic limit of the core's mass.

For disks with arbitrary values of $f_{\rm disk}$, the boundaries

$$a_{tg} = \begin{cases} 64 f_{\rm disk}^{-2}\eta_{\rm ice}\ {\rm AU} & \text{(the isolated core case)} \\ 9 f_{\rm disk}^{-2}\eta_{\rm ice}\ {\rm AU} & \text{(the nonisolated core case)} \end{cases} \quad (53)$$

and

$$a_{gi} = 5 f_{\rm disk}^{14/27}\left(\frac{\eta_{\rm ice}}{4}\right)^{10/27}\left(\frac{M_p}{4\ M_\oplus}\right)^{-10/81}\left(\frac{\tau_{\rm dep}}{10^7\ {\rm yr}}\right)^{-10/27}\ {\rm AU} \quad (54)$$

are set by the conditions $f_{\rm disk} = f_{tg}$ and f_{gi}, respectively. In massive disks with considerable heavy-elemental contents, $f_{\rm disk}$ may be considerably larger than unity. In these massive disks, a_{tg} is less than the ice boundary. In that case, it is

possible to form gas giants inside the ice boundary. In disks with $f_{\rm disk}$ smaller than a critical value

$$f_{\rm disk,\,min} = (0.9 \text{ or } 0.4)\left(\frac{\eta_{\rm ice}}{4}\right)^{-64/68} \times \left(\frac{M_p}{4\ M_\oplus}\right)^{5/102}\left(\frac{\tau_{\rm dep}}{10^7\ {\rm yr}}\right)^{5/34}, \quad (55)$$

$a_{gi} < a_{tg}$ (the factors 0.9 and 0.4 correspond to the isolated and nonisolated cases, respectively). These results are in agreement with the numerical results presented in Figures 6 and 7.

Since cores must attain at least 4 $M_\oplus$ before they can rapidly accrete gas, in metal-deficit disks with $f_{\rm disk} < f_{\rm disk,\,min}$, the gas giants cannot form. For a minimum-mass solar nebula model, $f_{\rm disk} \approx 1$ and is less than f_{tg} inside the ice line and greater than f_{gi} outside the ice line such that gas giants can only form at large radii. Since $f_{\rm disk,\,min}$ is smaller beyond the ice line, it sets a more stringent condition with $\eta_{\rm ice} = 4$. They are also consistent with the apparent paucity of metal-deficit stars with planets (e.g., Gonzalez 1997; Santos, Israelian, & Mayor 2001; Murray & Chaboyer 2002; Fischer & Valenti 2003).

In the gas giant formation domain, the total mass of the planets increases rapidly through runaway gas accretion after it exceeds $M_{c,\rm KH} \sim 4\ M_\oplus$. Gas accretion continues until the gas is depleted either globally or locally near the planets' orbits. Since the planets' growth timescale from the onset of rapid gas accretion to their asymptotic mass is relatively short compared with the disk depletion timescale, planets with $M_p \sim 10$–$100\ M_\oplus$ occupy a very limited domain inside $a \lesssim 3$ AU, as shown in Figures 6 and 7 (with the exception of the case where M_p is limited by $M_{g,\rm vis}$). In outer regions ($a \gtrsim 3$–10 AU), however, ice giants in such mass ranges can be formed. Their cores attain sufficient mass to accrete gas only after the gas has already been depleted severely.

4.2. *Prediction for Mass and Semimajor Axis Distribution*

Using the same theoretical model of core growth and gas accretion, we performed Monte Carlo calculations to produce a theoretical prediction for the M_p-a distribution of extrasolar planets to compare it with observations (Fig. 1). Planets are assumed to form with equal probability per interval of $\log a$. We assume the $f_{\rm disk}$ distribution as in Figure 8 to be consistent with observational data (Beckwith & Sargent 1996; Wyatt et al. 2003). This is a Gaussian distribution in terms of $\log_{10} f_{\rm disk}$ with a center at $\log_{10} f_{\rm disk} = 0.25$ and dispersion of 1.

We omit the high $f_{\rm disk}$ tail at $f_{\rm disk} > 30$, since such heavy disks are self-gravitationally unstable in outer regions. The gravitational stability parameter (Toomre 1964) for our disk models is

$$Q = \frac{c_s \Omega_{\rm K}}{\pi G \Sigma_g} \simeq 40 f_{\rm disk}^{-1}\left(\frac{a}{1\ {\rm AU}}\right)^{-1/4}. \quad (56)$$

The mass transfer associated with the gravitational instability would rapidly decrease local surface density Σ_g to a value such that $Q > 1$ (Lin & Pringle 1990; Nakamoto & Nakagawa 1994). However, if the disk is replenished by infall, modest Q-values (approximately a few) may be sustained for a timescale comparable to $\tau_{c,\rm acc}$. Nevertheless, surface density in outer regions ($a \gtrsim 10$ AU) in massive disks ($f_{\rm disk} \gtrsim 20$) may evolve. In principle, we should use the adjusted surface density

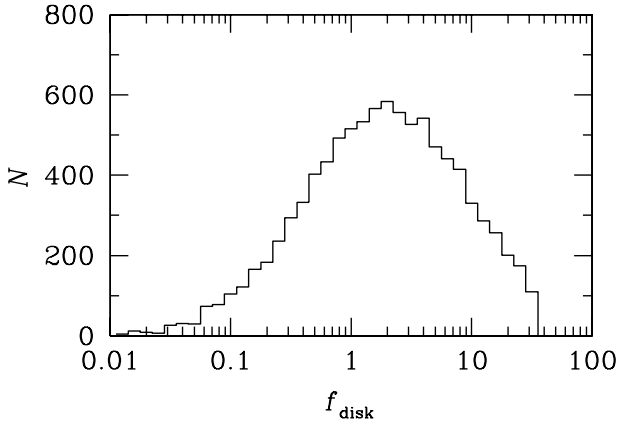

FIG. 8.—The $f_{\rm disk}$ distribution we use, which is a Gaussian distribution in terms of $\log_{10} f_{\rm disk}$ with a center at $\log_{10} f_{\rm disk} = 0.25$ and dispersion of 1. We omit the high $f_{\rm disk}$ tail at $f_{\rm disk} > 30$, since such heavy disks are self-gravitationally unstable.

distribution. Since most giant planets found in our model are formed at $a \lesssim 10$ AU, we adopt a simple cutoff at $f_{\rm disk} = 30$. We also examined a more artificial distribution in which $f_{\rm disk}$ is uniform in log scale from 0.1 to 30, but the results are almost the same.

The $\tau_{\rm disk}$ is distributed from 10^6 to 10^7 yr uniformly in log scale, which is also consistent with observational data (Beckwith & Sargent 1996; Wyatt et al. 2003). The range of stellar mass is also considered, so that $a_{\rm ice}$ is changed as equation (15). The location of $a_{\rm ice}$ is essential for the formation of gas giants, as shown before. In order to directly compare with the observed data, we adopt a similar selection criterion for M_* in the range of 0.7–1.4 $M_\odot$. Correspondingly, $a_{\rm ice} = 1.3$–5.3 AU. We also assume a uniform distribution in log scale for M_*. In each run, 10,000 initial conditions are taken.

We carry out calculations for planetary formation in disks with an evolving gas content. In these models, the cores' accretion is truncated when their masses have attained asymptotic values of $M_{c,\rm iso}$ (the results with $M_{c,\rm no\ iso}$ are similar). These results are shown in Figure 9. Three truncation asymptotic masses resulting from the truncation of gas accretion are considered: $M_{g,\rm iso}$ (Fig. 9*a*), $M_{g,\rm th}$ (Figs. 9*b* and 9*c*), and $M_{g,\rm vis}$ (Fig. 9*d*). We adopt $\Delta a_g = 2r_{\rm H}$ in Figure 9*a*, the critical Hill radius $r_{{\rm H},c}$ being h and $1.5h$ in Figures 9*b* and 9*c*, respectively, and $\alpha = 10^{-3}$ in Figure 9*d*.

In Figure 9, the green filled circles and blue crosses represent rocky and icy planets with an insignificant amount of gaseous envelopes around them. The green and blue open circles represent gas-rich rocky and icy planets with gaseous envelopes that are 1–10 times more massive than their cores. The red filled circles represent gas giants with gaseous envelopes more than 10 times more massive than their cores. The result in Figure 9*a* suggests that most gas giants form with masses an order of magnitude larger than Jupiter. Even larger masses would be obtainable if the gas accretion is unimpeded until M_p becomes $M_{g,\rm no\ iso}$ or $M_{g,\rm iso} + M_{g,\rm feed}$. This inconsistency with the observed mass distribution of the extrasolar planets is removed by the thermal gap formation condition as represented in Figures 9*b* and 9*c*. However, the viscous gap formation condition in Figure 9*d* places an overstrict upper limit on M_p so that gas giants cannot form. Numerical simulations of disk-planet interaction indicate that $M_{g,\rm th}$ is the

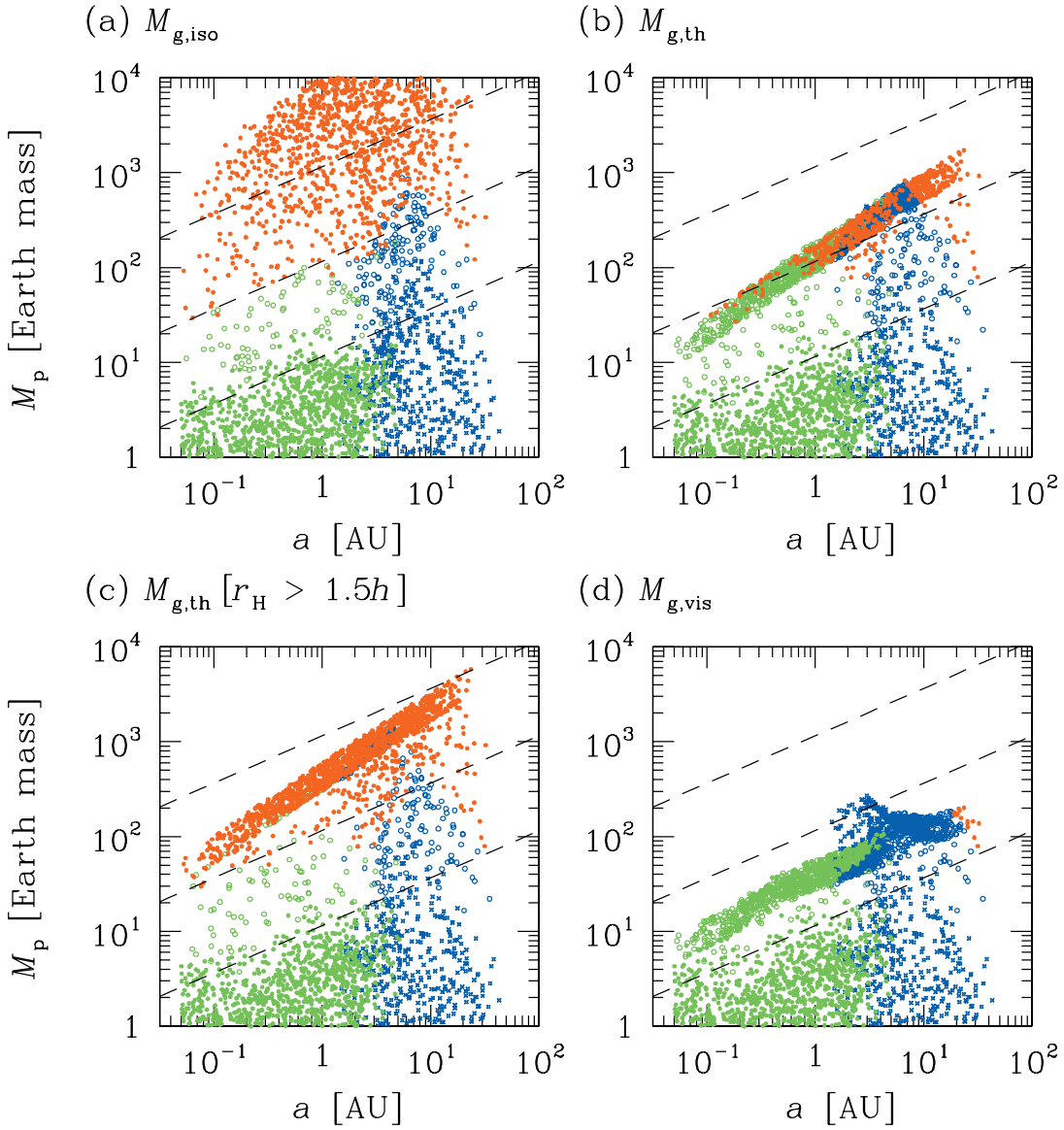

FIG. 9.—Theoretically predicted distribution based on the core accretion model for gas giant planets (for the range of parameters we used, see text). Cores are truncated by $M_{c,\rm iso}$. Gas accretion is truncated by (*a*) $M_{g,\rm iso}$, (*b* and *c*) $M_{g,\rm th}$, and (*d*) $M_{g,\rm vis}$. We adopt $\Delta a_g = 2r_{\rm H}$ in (*a*), the critical Hill radius $r_{{\rm H},c}$ being h and $1.5h$ in (*b*) and (*c*), respectively, and $\alpha = 10^{-3}$ in (*d*). The green filled circles and the blue crosses represent rocky and icy planets with gaseous envelopes less massive than their cores. The green and blue open circles represent gas-rich rocky and icy planets with gaseous envelopes that are 1–10 times more massive than their cores. The red filled circles represent gas giants with envelopes more massive than 10 times their cores. For comparison, we also plot observational data of extrasolar planets in (*d*). The dashed ascending lines correspond to radial velocity amplitude of 100 (*upper line*), 10 (*middle line*), and 1 m s^{-1} (*lower line*), assuming that the host star mass is 1 $M_\odot$.

appropriate upper limit for masses of gas giants (Bryden et al. 1999).

4.2.1. *Planet Desert*

In Figures 9*a*, 9*b*, and 9*d* these results show a deficit of planets with intermediate mass (10–100 $M_\oplus$) and semimajor axis less than 3 AU. The ranges of the deficit are different in Figures 9*a*, 9*b*, and 9*c*. The lower mass boundary of the planet-deficit domain in Figure 9 is demarcated by $M_p \sim 4\ M_\oplus$ for all models. This value of M_p simply corresponds to the minimum core mass that can satisfy both $M_c > M_{c,\rm crit}$ and $M_c > M_{c,\rm KH}$ (§ 3.1), which are the conditions for the cores to undergo rapid gas accretion. Transition across this boundary is weakened by the growth through giant impacts after the disk depletion. The truncation conditions of the cores and gas do not affect this boundary. Future observational determination of this lower mass boundary will provide useful information and constraints on the critical core mass that can lead to the onset of rapid gas accretion.

The upper mass boundary of the planet-deficit domain in Figure 9 is demarcated by the truncation condition for gas accretion. First, we consider the case of $M_{g,\rm iso}$. The upper mass boundary of the planet-deficit domain corresponds to the minimum asymptotic mass of gas giants. As shown in equation (50), in the case of core accretion being truncated by $M_{c,\rm iso}$, rapid gas accretion would occur if $f_{\rm disk} \gtrsim f_{tg} \simeq 8(a/1\ {\rm AU})^{-1/2}$.

In the inviscid gaseous disk model, the gas accretion process is terminated by isolation when the planets' mass reaches a value that is given by equation (36). Since $f_{g,0} = f_{\rm disk}$ in all the calculations described here, we obtain, by substituting f_{tg} into equation (36), a minimum truncated mass of gas giants in these regions to be

$$M^*_{g,\rm iso} \simeq 1.1 \times 10^3\ M_\oplus. \quad (57)$$

A similar calculation with $f_{tg} \simeq 3(a/1\ {\rm AU})^{-1/2}$ (for cores to be truncated by $M_{c,\rm no\ iso}$) yields

$$M^*_{g,\rm iso} \simeq 2.5 \times 10^2\ M_\oplus. \quad (58)$$

In regions of the disk where $f_{\rm disk} < f_{tg}$, cores cannot undergo rapid gas accretion, but in regions where $f_{\rm disk} > f_{tg}$, cores accrete gas until M_p reaches $M^*_{g,\rm iso}(f_{\rm disk}/f_{tg})^{3/2}$. The process of gas accretion can be stalled by the depletion of the disk gas. However, the timescale for the planets to attain their asymptotic masses is shorter than the gas depletion timescale, so that only a small fraction of planets may attain some intermediate masses. Therefore, most planets that undergo gas accretion have $M_p \gtrsim M^*_{\rm gas,iso}$, and $M^*_{g,\rm iso}$ corresponds to the upper mass boundary of the planet-deficit domain. Note that the a dependence vanishes in $M^*_{g,\rm iso}$, so that the upper mass boundary is essentially independent of a in Figure 9*a*. If asymptotic mass is regulated by $M_{g,\rm iso}$, the observed upper boundary of the planet-deficit domain would provide constraints on the feeding zone width (Δa_g) of gas giants and the critical surface density of solid components that can produce cores large enough for gas accretion (equivalently, f_{tg}).

4.2.2. *Asymptotic Mass of the Gas Giants*

Next, the results with gas truncation by $M_{g,\rm th}$ are considered. These conditions are particularly appropriate since the ongoing accretion from protostellar disks onto nearly all classical T Tauri stars clearly reflects the consequence of viscous transport of angular momentum and mass in the disks. The thermal truncation condition does not include an explicit $f_{\rm disk}$ dependence in the asymptotic mass of the gas giants. The mass dispersion of giant planets at given a is caused by the dispersion of the stellar mass M_* and is relatively small. The giant planet mass as a function of a clearly reflects the gap opening condition given by equation (38). The upper mass boundary of the planet-deficit domain, or equivalently the lower mass boundary of the giant planets' domain, is demarcated by $M_{g,\rm th}$ with $M_* \sim 0.7\ M_\odot$ in the present models. The truncation condition for the core growth stage does not affect the results. Note that we have adopted some idealized truncation conditions. In many numerical simulations (e.g., Artymowicz & Lubow 1996), there are indications that the gas flow onto the giant planets continues, albeit at some reduced rate, after the gap formation. Turbulence may be particularly important in sustaining the planets' growth until they have acquired larger masses than those shown in Figure 9*b*. In order to demonstrate this dependency, we consider in Figure 9*c* an additional model with $r_{{\rm H},c} = 1.5h$. This relaxed condition yields 3 times larger M_p for the gas giants.

The main difference between Figures 9*b* and 9*c* is the abundance of the green and blue open circles, which denote that the gas-rich terrestrial (rocky) planets and ice giants with the mass of the envelope do not exceed 10 times that of the core (i.e., $M_p < 10M_c$). From equations (21) and (38), we find

$$M_{g,\rm th} \simeq 0.75 \times 10^3 f_{\rm disk}^{-3/2} \eta_{\rm ice}^{-3/2} \left(\frac{r_{{\rm H},c}}{h}\right)^3 \left(\frac{M_*}{M_\odot}\right) M_{c,\rm iso}. \quad (59)$$

Although $\eta_{\rm ice} = 1$ inside the ice line, the critical value of $f_{\rm disk}$ ($\simeq$17) for $M_{g,\rm th} < 10M_{c,\rm iso}$ in Figure 9*b* (where $r_{{\rm H},c} = h$) is within the range of $f_{\rm disk}$ (0.1–30) we have adopted in our simulations. Outside the ice boundary where $\eta_{\rm ice} = 4$, it is much more likely that $M_{g,\rm th} < 10M_{c,\rm iso}$. Even though the masses of the gas-rich terrestrial planets and ice giants are dominated by their gaseous envelopes, the metallicity of their envelope may be greater than that of the disk. However, in Figure 9*c* where $r_{{\rm H},c} = 1.5h$, $M_{g,\rm th}$ is much larger than $M_{c,\rm iso}$. The asymptotic composition of the gas giants in these disks is diluted by the massive gaseous envelope.

4.2.3. *Radial Extent of Planet-forming Region*

The present scenario also indicates an outer boundary for the domain of gas or ice giant planet formation. The outer boundary for gas giants is set by a_{gi} (eq. [54]) where $3\tau_{c,\rm acc}(M_{c,\rm KH}) = \tau_{\rm disk}$. Although in equation (54) a_{gi} increases with $f_{\rm disk}$, it is limited to 30 AU even for the maximum value of $f_{\rm disk}$ (=30) we have adopted. This limited extent of the gas giant formation zone only applies to the core accretion scenario. In the gravitational instability scenario, gas giants are preferentially formed far from their host stars. The spatial distribution of gas giants may provide a discriminating test for the avenue of planet formation.

After the gas depletion, the residual rocky and icy embryos can grow through giant impacts. In the above discussions, we have already indicated that core growth is limited by (*a*) the availability of building block material (through $M_{c,\rm no\ iso}$; eq. [23]) and (*b*) the retention efficiency (through $M_{e,\rm sca}$; eq. [27]). However, even with unimpeded growth and infinite supply of planetesimals, (*c*) the maximum mass that can be attained within the life span of the host star (τ_*), through collisional coagulation, is (eq. [10])

$$M_{e,\rm life} \equiv M_e(\tau_*) \simeq 0.8 \times 10^4 \left(\frac{\tau_*}{1\ {\rm Gyr}}\right)^3 \left(\frac{\eta_{\rm ice}}{4}\right)^3 \times \left(\frac{f_{\rm disk}}{30}\right)^3 \left(\frac{a}{10\ {\rm AU}}\right)^{-9} M_\oplus. \quad (60)$$

The boundary between conditions (*a*) and (*b*) is demarcated by $M_{c,\rm no\ iso} = M_{e,\rm sca}$, and it occurs at

$$a_{ab} = 3\left(\frac{\eta_{\rm ice}}{4}\right)^{-1/2} \left(\frac{f_{\rm disk}}{30}\right)^{-1/2}\ {\rm AU}. \quad (61)$$

The boundary between conditions (*b*) and (*c*) is demarcated by $M_{e,\rm sca} = M_{e,\rm life}$, and it occurs at

$$a_{bc} = 24\left(\frac{\tau_*}{1\ {\rm Gyr}}\right)^{2/5} \left(\frac{\eta_{\rm ice}}{4}\right)^{2/5} \left(\frac{f_{\rm disk}}{30}\right)^{2/5}\ {\rm AU}. \quad (62)$$

Parameters $M_{e,\rm life}$ with $t = 1$ Gyr, $M_{c,\rm no\ iso}$, and $M_{e,\rm sca}$ are plotted as functions of a for $f_{\rm disk} = 1$, 3, 10, and 30 in Figure 10.

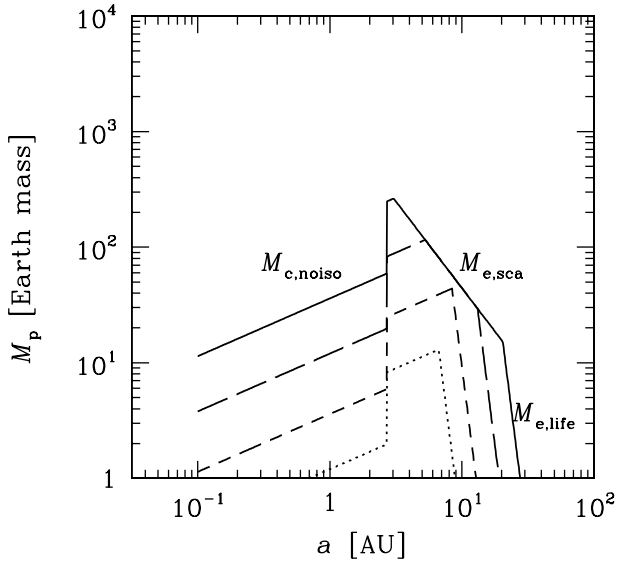

FIG. 10.—Limits of masses of rocky and icy planets. The masses are limited by the minimum of $M_{c,\mathrm{no\ iso}}$ (eq. [23]), $M_{e,\mathrm{sca}}$ (eq. [27]), and $M_{e,\mathrm{life}}$ with $t = 1$ Gyr (eq. [60]). The solid, long-dashed, short-dashed, and dotted lines express the cases of $f_{\mathrm{disk}} = 30$, 10, 3, and 1, respectively.

Rocky and icy planets can exit in the range surrounded by these masses. This analytic approximation is consistent with the upper limits of M_p shown in Figure 9. In all panels of Figure 9, the formation of both gas and ice giants is quenched beyond $\sim$30–40 AU despite the availability of planetesimal building blocks. In Figures 9*a*, 9*b*, and 9*c*, the gas-poor ice giants (represented by the blue crosses) do not extend above $\sim 20\ M_\oplus$. Their growth is limited mostly by $M_{e,\mathrm{life}}$. After the gas depletion, the enhanced velocity dispersion makes the accretion rate very low. In outer regions beyond $\sim$30–40 AU, this effect quenches ice giants' further growth. If the asymptotic mass of the giant planets is limited by the viscous condition (Fig. 9*d*), gas accretion beyond 10 AU would be quenched when $M_p \sim$ 40–100 $M_\oplus$. Since their growth is speeded up by the gas accretion, they may be able to attain masses larger than $M_{g,\mathrm{vis}}$ over some intermediate range of a (3–10 AU) through collisional coagulation after the gas depletion.

For modest values of f_{disk} such as that in the minimum-mass nebula model ($\sim$1), $a_{tg} < a_{gi} < a_{ab} < a_{bc}$. In this case, rocky, gas giant, and ice giant planets naturally form in order of increasing distance from their host stars. This expectation is consistent with the distribution of the planets in the solar system. Outside a_{ab}, the massive ice giants become the scattering agents that induce the residual planetesimals to be ejected to form cometary clouds and freely floating planets. This extrapolation is also consistent with the observed population of scattered Kuiper Belt objects (Duncan & Levison 1997). Beyond a_{bc}, the growth time is the limiting factor for the emergence of any sizeable protoplanets. In order to account for the absence of modest-size Kuiper Belt objects beyond $\sim$40–50 AU, $f_{\mathrm{disk}} \lesssim$ a few is required.

4.3. *Comparison with Observational Data*

The present observational data (Fig. 1) are obtained with some selection effects. For example, only planets with radial velocity amplitude $v_r \gtrsim 10$ m s^{-1} and semimajor axes $a \lesssim 4$–5 AU have been detected so far. The planets' mass inferred from these observations represents a set of minimum values, and their real magnitude is a function of the inclination angle of their orbital plane to the line of sight. Many planets are found with $a \sim 0.1$–1 AU and $M_p \gtrsim M_{\mathrm{J}}$. With the model in which the gas accretion is truncated by first isolation, we can construct such massive close-in planets (Fig. 9*a*), but their emergence requires massive disks that may be prone to gravitational instability. The second and third models (Figs. 9*b* and 9*c*) do not produce Jovian-mass planets inside $\sim$1 AU because the disks' aspect ratio is relatively small. There are many possibilities, within the framework of the core accretion scenario, to account for this discrepancy. Post–gap-opening accretion can lead to in situ formation of such planets. Orbital migration can also bring in the relatively massive planets formed in the outer regions where the disks' aspect ratio is relatively large (see next section).

The present data show an apparent lack of planets with $M_p \lesssim 200\ M_\oplus$ and $a \sim 0.2$–3 AU (see Fig. 1). When corrected for the inclination of their orbits, the demarcation boundary may be shifted to higher masses, by a factor of 2, from that indicated in Figure 1. If this hint of a planet-deficit domain is confirmed by the future observations, it would provide useful constraints on the truncation condition for gas accretion. At their face value, the present data are consistent with the simulated results with a combination of the isolation condition with $M_{\mathrm{gas,iso}}$ and the thermal condition with $M_{g,\mathrm{th}}$. The viscous condition with $M_{g,\mathrm{vis}}$ limits planet masses to values much smaller than observed masses unless (1) an extremely large value of α is taken (which can be ruled out by the persistent timescale of protostellar disks) or (2) accretion continues after gap formation.

Our numerical simulations also show an outer boundary for the planet-deficit domain at around 3 AU. This boundary reflects the changes in the dominant process that limits the formation of gas giants. At $a \lesssim 3$ AU, the condition of $M_c \gtrsim 4\ M_\oplus$ is more important because cores grow rapidly and reach their asymptotic mass prior to the era of gas depletion. However, at $a \gtrsim 3$ AU, the cores' growth is so slow that it is more important for $\tau_{c,\mathrm{acc}} \lesssim \tau_{\mathrm{disk}}$ to be satisfied. For most cores that can start gas accretion, $\tau_{c,\mathrm{acc}}$ is of order of τ_{disk}. Hence, many cores may not be able to initiate the process of gas accretion even though their mass can become larger than 10 $M_\oplus$ after gas depletion. As a result, planetary mass distribution at $a \gtrsim 3$ AU is likely to be continuous and does not show a clear deficit. Thus, the outer a boundary of the planet-deficit domain indicates the critical semimajor axis where core accretion timescales and disk gas depletion timescales are comparable.

5. ORBITAL MIGRATION

The existing data of known extrasolar planets include a population of short-period planets with period down to 3 days. We consider the possibility of orbital migration in this section.

5.1. *Model of Orbital Migration*

There are several suggestions that, as a result of a torque imbalance, embedded protoplanetary cores can undergo rapid type I migration (e.g., Goldreich & Tremaine 1980; Ward 1986). At 1 AU, the migration timescale for $M_c \sim 1\ M_\oplus$ is only 10^4–10^5 yr (Ward 1997; Tanaka et al. 2002; Bate et al. 2003). If type I migration is considered, all the protoplanetary cores have a tendency to rapidly migrate to the proximity of their host stars, prior to gas accretion. Thus, type I migration appears

to be inconsistent with prolific formation of extrasolar giant planets, as well as the efficient preservation of Earth-mass planets in the habitable zones around the Sun.

In contrast, type II migration naturally occurs when a planet acquires an adequate mass to open up a gap. Gap formation process itself requires the dissipation of tidally induced density waves. Turbulent viscosity is a possible mechanism to provide such a dissipation mechanism. It can also regulate the rate of gas accretion onto the classical T Tauri stars. Once a protoplanet has acquired an adequate mass to open up a gap, its orbital evolution is coupled with the viscous evolution of the disk (Lin & Papaloizou 1985).

In the next set of models, we include the effect of type II migration for gas giants that have already attained their asymptotic masses. For computational convenience, we introduce a simple prescription to follow the orbital evolution of the gas giant planets. The direction of the migration can be both inward and outward. We arbitrarily set a stopping semimajor axis for the inwardly migrating planets to be $\sim$0.04 AU. There are several potential mechanisms for halting the migration near the stellar surface (Lin, Bodenheimer, & Richardson 1996; Trilling et al. 1998), but none of these processes are effective beyond $\sim$0.1–0.2 AU. The migration can be halted beyond $\sim$0.1–0.2 AU by gas depletion (Trilling et al. 2002; Armitage et al. 2002; Matsuyama et al. 2003). However, both the planet formation and migration timescales at 0.2–3 AU are shorter than $\tau_{\rm disk} \sim 10^6$–$10^7$ yr. We consider below the necessary condition to build up gas giants and deplete the disk during the course of their migration so that they would be relocated to this intermediate location.

Here we consider only the type II migration in which orbital evolution of a planet embedded in a gap is coupled with the evolution of the disk (Lin et al. 1996; Trilling et al. 2002; Armitage et al. 2002). In a slowly evolving (quasi-steady) disk, the angular momentum flux due to the viscous stress is approximately independent of the disk radius. For a simple approximation, we estimate the net angular momentum transfer rate, in the absence of any planets, at the radius of maximum viscous couple R_m (e.g., Lynden-Bell & Pringle 1974),

$$\dot{J}_m \simeq \frac{3}{2}\Sigma_g \nu \Omega_{{\rm K},m} R_m^2 \simeq \frac{3\alpha}{2}\Sigma_{g,m} R_m^2 \Omega_{{\rm K},m}^2 h_m^2, \qquad (63)$$

where the subscript "m" denotes values of various quantities at R_m.

Across the gap, the planets' tidal torque regulates the angular momentum transport. When the disk inside their orbits is accreted onto their host stars or that outside their orbits diffuses to much larger radii, the embedded planets maintain the angular momentum transport balance $\frac{1}{2}M_p\Omega_{{\rm K},p}a_p\dot{a}_p \sim \dot{J}_m$ by adjusting their orbital radius a_p (Lin & Papaloizou 1985; Lin et al. 1996). This process leads to planetary migration on a rate

$$\frac{\dot{a}_p}{a_p} \simeq 3\,{\rm sign}\left(a_p - R_m\right)\alpha \frac{\Sigma_{g,m}R_m^2}{M_p}\frac{\Omega_{{\rm K},m}}{\Omega_{{\rm K},p}}\left(\frac{h_m}{a_p}\right)^2 \Omega_{{\rm K},m}, \qquad (64)$$

where $\Omega_{{\rm K},p}$ is Kepler frequency of the planet's orbit at a_p.

The sign implies that after it has opened up a gap, an embedded planet at radius a_p would migrate with the disk gas toward its host star if $a_p < R_m$ and away from the star if $a_p > R_m$. Using equations (16) and (12) to substitute for Σ_g and h, we obtain a migration timescale

$$\tau_{\rm mig} = \frac{a_p}{|\dot{a}_p|} = 0.8 \times 10^6 f_g^{-1}\left(\frac{M_p}{M_{\rm J}}\right)\left(\frac{M_\odot}{M_*}\right) \times \left(\frac{\alpha}{10^{-4}}\right)^{-1}\left(\frac{a_p}{1\ {\rm AU}}\right)^{1/2}\ {\rm yr}. \qquad (65)$$

5.2. *An α-Prescription for Gas Disk Evolution*

The value of R_m depends on the Σ_g distribution. For the minimum-mass solar nebula model, we estimate it to be $\sim$10 AU (Lin & Papaloizou 1985). However, the observationally inferred size and mass of the disks have a large dispersion. A similar dispersion is expected in R_m. During the viscous diffusion process, R_m evolves outward if there is no infall to replenish the disk mass. In the absence of infall and outflow, Σ_g declines in most parts of the disk as mass is accreted onto the host stars. From the conservation of the total disk mass,

$$J_{\rm tot} \sim \pi \Sigma_g R_m^4 \Omega_{{\rm K},m}, \qquad (66)$$

we expect

$$\frac{\dot{R}_m}{R_m} \sim -\frac{2\dot{\Sigma}_g}{5\Sigma_g}. \qquad (67)$$

If the disk depletion is mostly driven by photoevaporation or stellar wind ablation, the expansion rate of R_m would be slower. However, as shown in equation (64), in the model with $\Sigma_g \propto a^{-3/2}$ and $h \propto a^{5/4}$ (equivalently, $T \propto a^{-1/2}$), the planetary migration rate is independent of R_m except for outer regions ($a \gtrsim R_m$) where the direction of migration is outward. Hence, we only need an approximate prescription for the time evolution of R_m in our simulation. Corresponding to equations (48) and (67), we set

$$R_m = 10 \exp\left(\frac{2t}{5\tau_{\rm disk}}\right)\ {\rm AU}. \qquad (68)$$

In a quasi–steady state, the radial velocity of the gas is

$$u_r \simeq -\frac{3}{2}\frac{\nu}{a_p} \simeq -\frac{3\alpha}{2}\left(\frac{h_{\rm p}}{a}\right)^2 a_p \Omega_{{\rm K},p}, \qquad (69)$$

in regions well inside R_m. The scale h_p is evaluated at a_p. Note that $|\dot{a}_p|$ cannot be faster than $|u_r|$. Equivalently, $\tau_{\rm mig}$ cannot be smaller than

$$\tau_{{\rm disk,\,acc}} = \frac{a_p}{|u_r|} \simeq 4.3 \times 10^5 \left(\frac{\alpha}{10^{-4}}\right)^{-1}\left(\frac{a_p}{1\ {\rm AU}}\right)\ {\rm yr}. \qquad (70)$$

For small planets embedded in relatively massive disks, $\tau_{\rm mig}$ is limited by $\tau_{{\rm disk,\,acc}}$. In addition, when a_p decreases to 0.04 AU, migration is halted as mentioned above.

Integrating $\dot{a}_p$ with equations (65) and (68), we show examples of type II migration with our model in Figure 11, where time is scaled by $\tau_{\rm mig}$ at 1 AU ($\tau_{{\rm mig},1}$). At $a \sim 1$ AU, planets can migrate by a significant distance in the limit that $\tau_{\rm dep} \gtrsim \tau_{{\rm mig},1}$. Since $\tau_{\rm mig} \propto a_p^{1/2}$, the inner planets tend to migrate

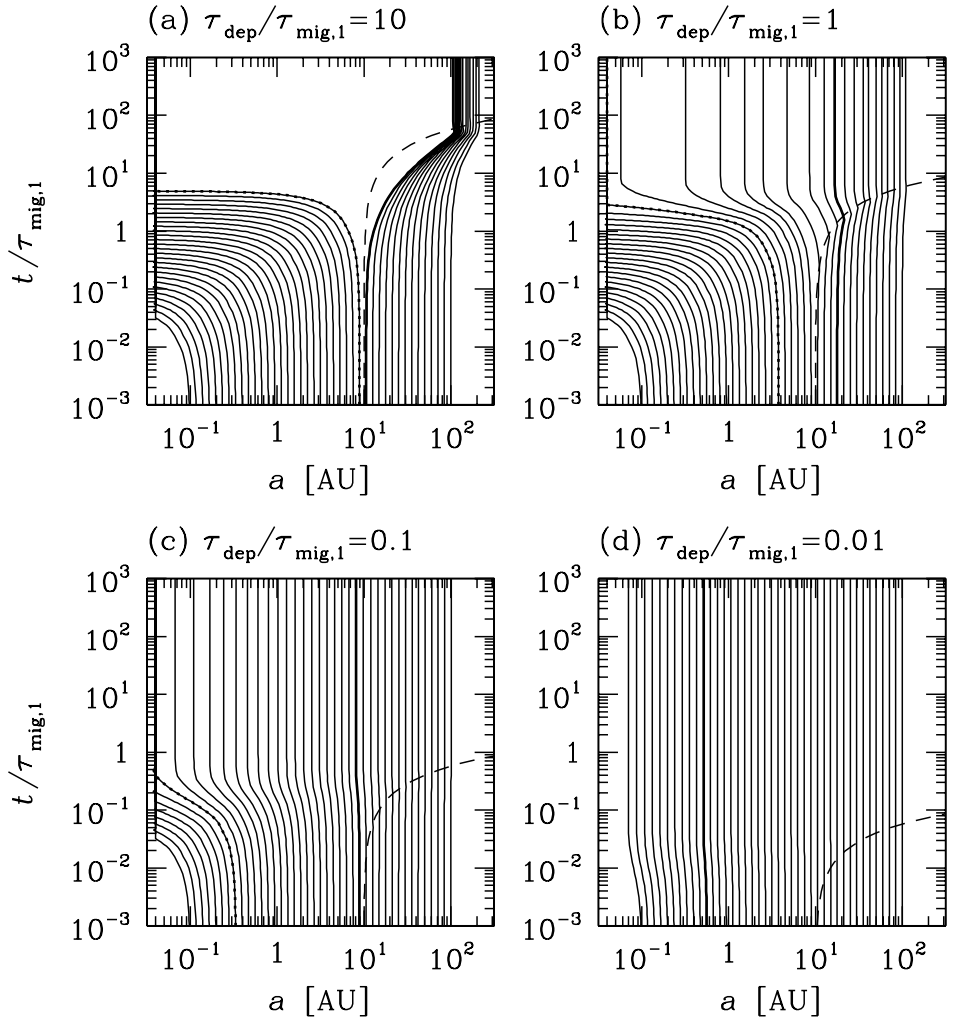

FIG. 11.—Planetary migration obtained by integrating $\dot{a}_p$ with eqs. (65) and (68), shown by solid lines. Inside the thick dashed lines, final semimajor axes reach 0.04 AU. They are greater than 0.9 times their original locations, outside the thick solid lines. Dashed lines express R_m. Time is scaled by τ_{mig} at 1 AU ($\tau_{mig,1}$).

over a greater radial extent and the inward migration accelerates with time. In all figures, we indicate the evolution of R_m with dashed lines. Planets outside R_m migrated outward. Some planets that formed slightly outside the initial R_m migrate outward first. However, as R_m expands beyond their orbits, their migration reverses direction and they undergo orbital decay (Lin & Papaloizou 1985). The migration of some planets is stalled at intermediate radii when the disk is depleted. Note that the number of planets that stalled with intermediate semimajor axes or equivalently periods is a function of $\tau_{dep}/\tau_{mig,1}$. The initial migration timescale at 1 AU, $\tau_{mig,1}$, provides an arbitrary fiducial comparison between the disk depletion and planets' migration timescales. In models with $\tau_{dep}/\tau_{mig,1} > 1$, delicate timing is needed for a few planets to stall their orbital evolution at a fraction of an AU. This result is similar to those found by Trilling et al. (2002) and Armitage et al. (2002). However, in models with relatively small $\tau_{dep}/\tau_{mig,1}$, a significant fraction of the gas giant planets formed near 1 AU may attain asymptotic semimajor axes between 0.04 and 1 AU.

In Figure 11 we highlight the critical migration paths of (1) those planets that marginally migrate from an initial semimajor axis a_1 to 0.04 AU and (2) those planets that attain an asymptotic semimajor axis that is greater than 0.9 times that of their initial semimajor axis a_2. Since planets that form with semimajor axis between a_1 and a_2 attain asymptotic a-values between 0.04 AU and $\sim a_2$, relatively large values of $\tau_{dep}/\tau_{mig,1}$ would lead to a significant modification in the semimajor axis distribution of the planets.

5.3. *The Modification of the Semimajor Axis Distribution by Migration*

We apply the above prescription for migration to the planetary growth model. We added the effects of migration to the Monte Carlo calculations in § 4.2 (Figs. 9*a*, 9*b*, and 9*c*). We assume that type II migration starts when a planet's mass reaches $M_{g,th}$ and a gap is opened up in the nascent disk near its orbit (models [*a*] and [*b*]). In the case that the gas truncation is induced by isolation, it is less clear when type II migration would be initiated. For simplicity, we assume that migration starts when planetary mass reaches $M_{g,iso}$, which is larger than $M_{g,th}$. For model (*c*), migration is initiated when r_H becomes larger than $h/1.5$ such that there is a range for which gas accretion and migration occur concurrently. This migration condition is similar to $M_p > M_{g,vis}$. (As mentioned in the

last section, the gas truncation by $M_{\rm gas,\,vis}$ seems to be inconsistent with the observational data, but the migration condition by $M_{\rm gas,vis}$ may be reasonable.)

In these calculations, $\tau_{\rm dep} = 10^6$–10^7 yr. The time-dependent calculation of disk evolution (Lynden-Bell & Pringle 1974) indicates that the disk mass declines on the viscous diffusion timescale near R_m. If gas depletion in disks is due to their viscous evolution, we would expect $\tau_{\rm dep}$ to be comparable to $\tau_{\rm disk,\,acc}$ (eq. [70]) near $R_m \sim 10$ AU. In order to match the observed properties of protostellar disks around classical T Tauri stars, we adopt $\alpha = 10^{-4}$, which corresponds to $\tau_{\rm dep}/\tau_{\rm disk,\,acc} \sim 1$ at 10 AU.

The results of our simulations are shown in Figure 12 for three series of models. In each case, the gas and core accretion are truncated by the conditions that correspond to those in Figure 9. The results show that the spatial distribution of the gas-poor cores is not affected by the migration because it only affects those planets that are able to accrete gas and to open up gaps. But for gas giant planets, equation (65) indicates that the migration timescale increases with their masses and semimajor axes. The less massive gas giants are formed preferentially with relatively small semimajor axes, and they migrate to $\sim$0.04 AU in all the cases. This result is consistent with the observed mass distribution of the short-period planets, which appears to be smaller than that of planets with periods longer than a few months (Udry et al. 2003).

Gas giant planets with $\tau_{\rm mig} \lesssim \tau_{\rm disk}$ migrate over extended radial distance provided that the disk gas is preserved for a sufficiently long time for them to form. For example, the critical value of $f_{\rm disk}$ for the formation of gas giants is $\sim$3–8 at $a \sim 1$ AU where $\eta_{\rm ice} = 1$ (see § 4.1). From equation (18), we find that in disks with $f_{\rm disk}$ larger than the critical value, the

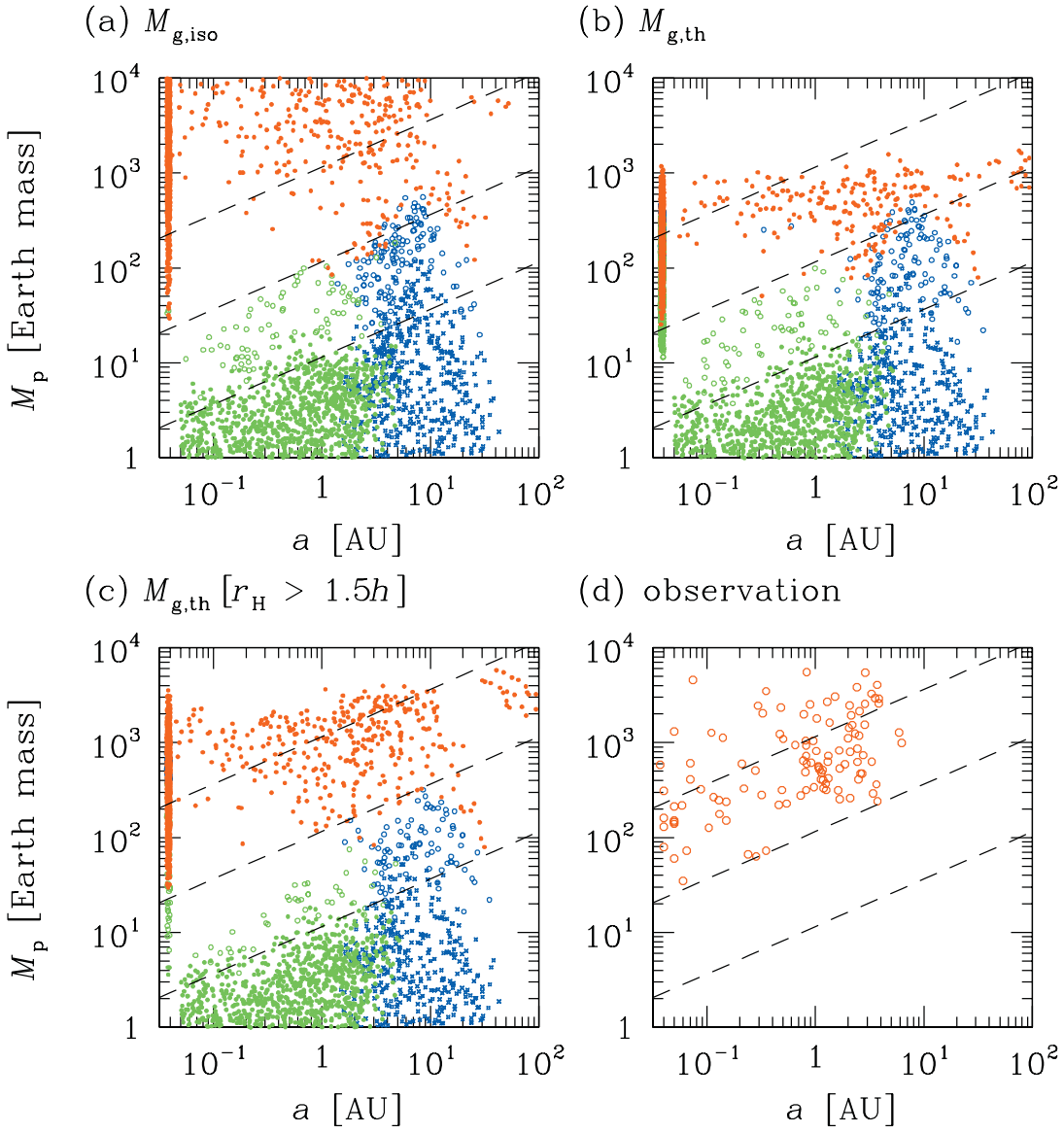

FIG. 12.—Similar plots as Fig. 9, but with the effect of type II migration included. The value of α-viscosity is taken as $\alpha = 10^{-4}$ to be consistent with disk depletion times $\sim 10^6$–10^7 yr. (*a*) Gas accretion is truncated by $M_{g,\rm iso}$ and core accretion by $M_{c,\rm iso}$; (*b*) $M_{g,\rm iso}$ and $M_{c,\rm no\,iso}$; (*c*) $M_{g,\rm th}$ and $M_{c,\rm iso}$. We adopt $\Delta a_g = 2r_{\rm H}$ in (*a*) and $M_* = 1\ M_\odot$ in (*c*).

timescale for a core to acquire a mass $M_p \gtrsim 4\ M_\oplus$ is $3\tau_{c,\rm acc} \lesssim 10^5$ yr, which is much smaller than the mean disk depletion timescale $\tau_{\rm disk} \sim 10^6$–$10^7$ yr. If the subsequent gas accretion is limited by either $M_{g,\rm th}$ or $M_{g,\rm iso}$, the asymptotic mass of the gas giant would be $\lesssim 10 M_{\rm J}$ (Fig. 9). For this range of M_p and $f_{\rm disk}$, we find, from equations (65) and (70), that the migration timescale $\tau_{\rm mig}$ is less than a few million years provided $\alpha \sim 10^{-4}$. In most disks, $R_m \gg 1$ AU so that the planets formed at $a \sim 1$ AU have $\tau_{c,\rm acc} \lesssim \tau_{\rm mig} \lesssim \tau_{\rm disk}$. Thus, within our model here, most gas giant planets formed within $\sim$1 AU are removed by the orbital migration independent of the truncation condition for gas accretion.

Nevertheless, there is a population of gas giants that attain an asymptotic semimajor axis in the range of a fraction of an AU. In fact, the distribution of semimajor axis is nearly continuous from $\sim$0.04 to 4 AU. As we have indicated in the discussion of Figure 11, planets formed between a_1 and a_2 slightly outside the initial radius of maximum viscous stress (R_m) migrate outward first. They reverse their direction and migrate inward after R_m has expanded beyond their orbit. (In all our calculations, we adopt $R_m = 10$ AU initially so that $a_1 \sim 3$–5 AU and $a_2 \sim 10$ AU.) Their period distribution in the range of a few weeks to years is determined by the ratio of the disk depletion and viscous timescales. With our adopted value of $\tau_{\rm dep}/\tau_{\rm disk,\,acc}$ ($\simeq$1), the simulated a distribution is similar to that observed.

Numerical simulations of disk-planet interaction suggest that there may be lingering gas accretion after the gap formation that may lead to M_p being somewhat but not substantially larger than $M_{g,\rm th}$. The postformation accretion may be particularly effective for the eccentric planets because their large epicyclic excursion can be extended beyond the boundaries of the gap. From equation (65) we find that $\tau_{\rm mig} \simeq \tau_{\rm disk}$ when M_p reaches

$$M_{\rm mig} = 12.5 f_g \left(\frac{\tau_{\rm disk}}{10^7\ {\rm yr}}\right)\left(\frac{M_*}{M_\odot}\right)\left(\frac{\alpha}{10^{-4}}\right)\left(\frac{a}{1\ {\rm AU}}\right)^{-1/2} M_{\rm J}. \quad (71)$$

If such an effect leads to the formation of any massive planets with $M_p > M_{\rm mig}$, they would not be able to migrate significantly from their birth place.

5.4. *Preservation of the Planet-Deficit Domain*

The results in Figure 12 show that the domain of the planet desert becomes more clearly defined with all three prescriptions for the truncation of gas accretion. In comparison with the planets' initial properties (see Fig. 9), the effect of the orbital migration is to reduce and erase the differences introduced to the M_p-a distribution by the different truncation conditions for gas accretion.

In this series of simulations, we only consider type II migration, which occurs only if a planet can open up a gap with a mass in excess of $(0.3 - 1)M_{g,\rm th}$ [$\sim(30$–$10^2)(a/1\ {\rm AU})^{3/4}\ M_\oplus$]. The lower M_p boundary of the planet desert is not modified by the type II migration process because it is populated by cores that have not yet initiated the process of rapid gas accretion and may not migrate. As we have already shown that this boundary is primarily determined by the cores' mass required for transition from the predominantly planetesimal to the mostly gas accretion, it is insensitive to the truncation condition for the cores and their asymptotic masses.

A direct comparison between Figures 9 and 12 clearly indicates that the planet migration process significantly alters the upper M_p boundary of the planet-deficit domain. Gas giants formed with $a < a_1 \sim 3 - 5$ AU (see Fig. 12) migrate to 0.04 AU, but some planets formed between a_1 and $a_2 \sim 10$ AU attain asymptotic a between 0.04 and 4 AU. As the semimajor axes of these marginally survivable gas giants spread out, they attain a nearly logarithmic period distribution similar to the observed period distribution. Outside a_2, the gas giants form in the advanced stages of disk evolution when there is insufficient gas to induce any significant migration. Based on the results in Figure 12, we infer a substantial upturn in the semimajor axis distribution of Jupiter-mass gas giants at around 10 AU. The boundary of the upturn in the period distribution is determined by the ratio of gas depletion and the viscous evolution timescales of the disk.

During the migration, the gas giants are not expected to lose mass. Thus, the upper M_p boundary of the planet-deficit region is set by the lowest gas accretion truncation mass between a_1 and a_2. Above this upper boundary, the spread in M_p among the gas giants with any given a is due to the dispersion in the gas accretion truncation condition induced by the mass range of the host stars and nascent disks.

In this series of simulations, the outer a boundary of the planet desert in the M_p-a diagram occurs at $\sim$3 AU for all three classes of models. The magnitude of the outer a boundary is determined by the location where cores can attain a sufficient mass to undergo efficient gas accretion prior to the depletion of the gas in the disk. Since this condition is associated with the evolution of the cores, the location of the outer a boundary does not depend on either the gas accretion truncation conditions or the migration process.

Beyond the outer a boundary, ice giant planets, similar to Uranus and Neptune, can form with 10–100 $M_\oplus$. In these regions, the cores grow relatively slowly. Even though the asymptotic mass of the cores is relatively large, they are unable to acquire $M_{c,\rm KH} \sim 4\ M_\oplus$ to initiate a phase of rapid gas accretion. The large asymptotic mass of these planets is acquired during the final phase of their assemblage after gas in the disk has been depleted. In the limit that some residual gas in the disk is preserved for an extended length of time, type II migration cannot relocate these planets because their mass is too small to open up a gap. Nevertheless, the mass spectrum at any a beyond the outer boundary of the planet desert can evolve slightly with gas accretion and significantly via residual core accretion and giant impacts. The timescale of growth through giant impacts is similar to that for the oligarchic cores and is an increasing function of the planets' mass. This further coagulation process leads to a continuous mass spectrum. The range of ice giants' masses in the region just beyond the outer a boundary is determined by the dispersion in the heavy-element content, i.e., $f_{\rm disk}$, out there.

The center of the planet-deficit domain is not entirely void of planets with intermediate M_p and a-values. Within the present theoretical framework of our models, only type II migration can modify the planets' semimajor axis. However, the necessary condition for type II migration is for gas giants to reach their gas accretion truncation mass $M_{g,\rm th}$, which is an increasing function of a. Gas giants with M_p less than the local $M_{g,\rm th}$ can be formed inside any disk location. However, planets formed inside the radius of maximum viscous stress in the disk R_m must always migrate inward. Since R_m is generally comparable to or larger than a_2, planets with intermediate M_p and a cannot migrate into the planet desert domains from

smaller or larger a-values. In our simulation, a few planets located in the planet-deficit, intermediate M_p and a region can be formed in marginally massive disks where $f_{\rm disk} > f_{\rm disk,\,min}$ and $f_g \sim (M_p/M_{\rm J})(a/1\ {\rm AU})^{-1/2}$ (see eqs. [55] and [47]). In this estimate, we assume that since these planets do not have adequate mass to open a gap, they eventually acquire all the nearby residual disk gas.

5.5. *The Spatial Extent of Planetary Systems*

In the scenario we presented here, we artificially halt the migration at 0.04 AU to represent the effect of tidal and magnetospheric interaction between short-period planets and their host stars. Besides these processes, MHD turbulence in the disk may also play a role in halting their migration (Terquem 2003). Since most of the short-period planets were formed with $a < a_1$, they generally form with less mass than the planets that accreted gas later, at larger disk radii, and retained a greater fraction of their original semimajor axis. Most gas giant planets formed inside a_1 migrate to 0.04 AU. Since gas giants can readily form well within a_1 (see Fig. 9), a large accumulation of short-period planets is expected. Although there is a spike in the observed period distribution just outside 0.03 AU, the amplitude of this enhancement is modest. Near the surface of the host stars, the combined effects of tidal, magnetospheric, and radiative effects of the host stars, as well as the secular perturbation of more distant planets, disks, and stars, may lead to the destruction of the short-period planets and the disruptions of their orbits. For our results in Figure 12 to be consistent with the observed distribution, 90%–95% of the planets that migrate to within 0.05 AU must perish.

For the outer boundary of planetary systems, we find that there are several very massive planets that managed to migrate to $a \sim 50$–100 AU in Figures 12*a*, 12*b*, and 12*c*. These planets were formed at 10–30 AU, just outside a_2 in massive disks we have simulated. With their large values of $a \sim 10$–30 AU and $f_{\rm disk} \sim 20$–30, the gravitational stability parameter Q (eq. [56]) at formation locations of these planets is found to be 0.7–1.2, which may be (marginally) gravitationally unstable. Hence, the outward-migrating massive gas giants may actually be more rare.

For disks with modest masses, ice giants can accrete gas to form sizable gaseous envelopes (represented by open blue circles) well beyond the ice boundary. We assume that the ice giants do not migrate because they do not have a sufficient mass to open a clean gap. Nevertheless, the weak tidal interaction may be adequate to induce the ice giants to migrate primarily outward over a limited extent. In the solar system, the migration of Neptune over several AU on a timescale of $\sim$10 Myr may have led to the capture of Kuiper Belt objects on its 3 : 2 (but not on its 2 : 1) mean motion resonances (Ida et al. 2000).

In the current analysis, we do not consider the interaction between multiple planets that can lead to dynamical instabilities (Chambers, Wetherill, & Boss 1996; Lin & Ida 1997; Marzari & Weidenschilling 2002). Although sizeable planets may be ejected to large distances from their host stars, such an instability is likely to induce the orbits of the residual planets to become highly eccentric and dynamically segregated with large ($\gtrsim$10) period ratios (e.g., Weidenschilling & Marzari 1996; Lin & Ida 1997). The search for the orderly packed ice giants with nearly circular orbits may provide useful constraints to differentiate the core accretion and gravitational instability scenarios for planet formation.

6. SUMMARY AND DISCUSSIONS

We have investigated the mass and semimajor axis distributions of extrasolar planets through theoretical models based on the core accretion model for formation of gas giants. Core accretion from planetesimals is modeled by the results of N-body simulations. Gas accretion onto the cores is modeled with Kelvin-Helmholtz contraction of the gas envelope. Since the termination of gas accretion onto cores has some uncertainty, we considered various models for the asymptotic mass of the gas giants. In some calculations, we also include the effects of type II migration.

In general, the formation of gas giants is favored just outside the ice boundary at $\sim$3 AU. Inside the ice boundary, because the volatile gases cannot condense into grains, the mass of solid cores tends to be smaller than 4 $M_\oplus$, which is necessary for the onset of rapid gas accretion onto them. On the other hand, in outer regions ($\gtrsim$10 AU), core accretion is so slow that cores cannot attain 4 $M_\oplus$ before the disk gas is depleted on the timescale of $\sim 10^6$–10^7 yr. In very massive disks, however, cores become massive enough for the onset of rapid gas accretion even inside the ice boundary within the disk lifetime to attain gas mass $\gtrsim$100 $M_\oplus$. Since planets grow very rapidly from 10 to 100 $M_\oplus$, planets of the intermediate masses are rare at $a \lesssim 3$ AU (planet desert). If the effect of type II migration is included, the deficit becomes more clear and tends to become independent of the model of termination of gas accretion. It also results in accumulation of planets at $a \sim 0.03$–0.1 AU. As a result, the deficit becomes $\sim$10–100 $M_\oplus$ and 0.2–3 AU.

The current radial velocity survey of nearby stars is limited by the availability of accurate radial velocity measurements (down to the level of $v_r \gtrsim 10$ m s^{-1}) over the past few years. Planets with masses comparable to that of Jupiter and $a \lesssim 4$–5 AU are inferred from these observations. The processed data show a hint of the planet desert (Fig. 1). Further observations in the regime of longer periods (larger a) and smaller v_r will clarify the existence of a planet desert (a deficit of planets with intermediate mass and semimajor axis planets).

Gas giants could also be formed by self-gravitational collapse of a disk (e.g., Boss 2001). If extrasolar planets are formed from the self-gravitational collapse, the mass and semimajor axis distributions of extrasolar planets should show very different features from those we show here based on the core accretion model for gas giants. As we showed in §§ 4 and 5, with the core accretion model, gas giants may be limited to the regions $a \lesssim 20$ AU, except for planets on eccentric orbits that are scattered from inner regions by dynamical instabilities in multiple gas giant systems (which we do not consider in this paper). On the other hand, in the self-gravitational collapse model, gas giants are preferentially formed far from their host stars (see eq. [56]), although the mass distribution of gas giants is not clear. The search for gas giants on nearly circular orbits beyond 20–30 AU may provide useful constraints to differentiate the core accretion and gravitational instability models for formation of gas giants.

If the presence of a planet desert is confirmed by future observations, the boundaries of the planet-deficit domain in the mass and semimajor axis plane should provide the following constraints on the planetary formation processes (see also Fig. 13):

1. The lower mass boundary (M_l) indicates the core mass that can initiate the onset of rapid gas accretion. Our theoretical model predicts that $M_l \sim 4\ M_\oplus$ and it does not depend on a. (If

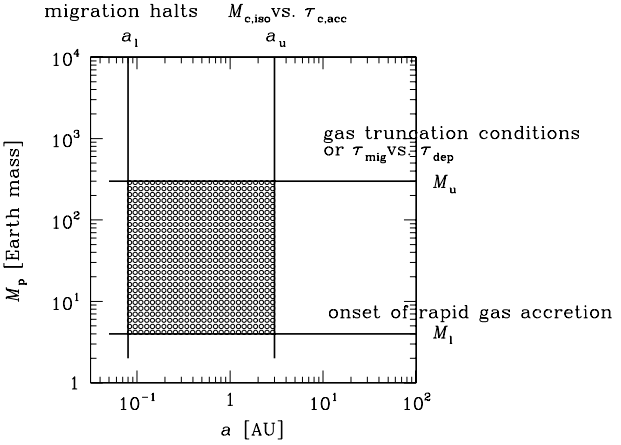

FIG. 13.—Illustrative figure for the planet desert. The lower mass boundary (M_l) indicates the core mass that can initiate the onset of rapid gas accretion. The upper mass boundary (M_u) and its dependence on a provide clues on the truncation mechanism of gas accretion. The smaller a boundary (a_l) indicates the maximum radius at which type II migration can be halted. The larger a boundary (a_u) traces out the radius where a dominant condition for formation of gas giants changes between the $\tau_{c,\mathrm{acc}}$ condition and $M_{c,\mathrm{iso}}$ condition. For details, see text.

we include the coalescence between cores after gas depletion, M_l slightly increases with a.)

2. The value of the upper mass boundary (M_u) and its dependence on a provide clues on the truncation mechanism of gas accretion. For various models we find (1) $M_u = 3 \times 10^2$–$10^3\ M_\oplus$ (and independent of a) if the gas giants' growth is limited by an isolation process, (2) $M_u = 20(\alpha/10^{-3})(a/1\ \mathrm{AU})^{1/2}\ M_\oplus$ if a complete gap is formed through the viscous condition, or (3) $M_u = 80(a/1\ \mathrm{AU})^{3/4}\ M_\oplus$ if it is due to the thermal condition. However, if the effect of type II migration is included, the results in models 1 and 3 lead to similar M_p-a distribution. Then the magnitude of M_u constrains the migration timescales and disk depletion timescales.

3. The smaller a boundary (a_l) indicates the maximum radius at which type II migration can be halted.

4. The larger a boundary (a_u) traces out the radius where a dominant condition for formation of gas giants changes between the $\tau_{c,\mathrm{acc}}$ condition and $M_{c,\mathrm{iso}}$ condition. At $a \gtrsim a_u$, the former is more important than the latter, and vice versa. Our theoretical model predicts that $a_u \sim 3$ AU.

The results presented here show that the sequences of rocky (terrestrial), gas giant, and ice giant planets are clearly segregated in the M_p-a diagram. The importance of this diagram to planet formation is similar to that of the color-magnitude diagram for stellar evolution. Comparison of future observations and more refined theoretical models will reveal the formation processes of extrasolar planets. In the near future our inability to directly detect the presence of terrestrial planets limits the comparison to only the giant planet population. In follow-up papers, we will consider a wider variety of models and identify some robust constraints. Our eventual objective is to extrapolate the ubiquity of rocky planets and formulate a predictable theory of planet formation from the statical properties of the giant planets.

We thank E. Kokubo, M. Ikoma, and G. Laughlin for useful discussions. This work is supported by NASA through NAGS5-11779 under its Origins program, JPL 1228184 under its SIM program, and NSF through AST 99-87417.

REFERENCES

Aarseth, S. J., Lin, D. N. C., & Palmer, P. L. 1993, ApJ, 403, 351
Adachi, I., Hayashi, C., & Nakazawa, K. 1976, Prog. Theor. Phys., 56, 1756
Armitage, P. J., Livio, M., Lubow, S. H., & Pringle, J. E. 2002, MNRAS, 334, 248
Artymowicz, P. 1993, ApJ, 419, 166
Artymowicz, P., & Lubow, S. H. 1996, ApJ, 467, L77
Balmforth, N. J., & Korycansky, D. G. 2001, MNRAS, 326, 833
Bate, M. R., Lubow, S. H., Ogilvie, G. I., & Miller, K. A. 2003, MNRAS, 341, 213
Beckwith, S. V. W., & Sargent, A. I. 1996, Nature, 383, 139
Bodenheimer, P., & Pollack, J. B. 1986, Icarus, 67, 391
Bondi, H. 1952, MNRAS, 112, 195
Boss, A. P. 2001, ApJ, 551, L167
Bryden, G., Lin, D. N. C., & Ida, S. 2000a, ApJ, 544, 481
Bryden, G., Rzyczka, M., Lin, D. N. C., & Bodenheimer, P. 2000b, ApJ, 540, 1091
Bryden, G., Xingming, C., Lin, D. N. C., Nelson, R., & Papaloizou, J. C. B. 1999, ApJ, 514, 344
Calvet, N., Hartmann, L., & Strom, S. E. 2000, in Protostars and Planets IV, ed. V. Mannings, A. P. Boss, & S. S. Russell (Tucson: Univ. Arizona Press), 377
Cameron, A. G. W., & Ward, W. R. 1976, Lunar Planet. Sci. Conf., 7, 120
Chambers, J. E., Wetherill, G. W., & Boss, A. P. 1996, Icarus, 119, 261
D'Alessio, P, Calvet, N., & Hartmann, L. 2001, ApJ, 553, 321
Duncan, M. J., & Levison, H. F. 1997, Science, 276, 1670
Duvert, G., Guilloteau, S., Ménard, F., Simon, M., & Dutrey, A. 2000, A&A, 355, 165
Fischer, D. A., & Valenti, J. A. 2003, in ASP Conf. Ser. 294, Scientific Frontiers in Research on Extrasolar Planets, ed. D. Deming & S. Seager (San Francisco: ASP), 117
Goldreich, P., & Tremaine, S. 1980, ApJ, 241, 425
Gonzalez, G. 1997, MNRAS, 285, 403
Greenberg, R., Hartmann, W. K., Chapman, C. R., & Wacker, J. F. 1978, Icarus, 35, 1
Gu, P., Lin, D. N. C., & Bodenheimer, P. H. 2003, ApJ, 588, 509
Haisch, K. E., Lada, E. A., & Lada, C. J. 2001, ApJ, 553, L153
Halliday, A. N., Lee, D.-C., & Jacobsen, S. B. 2000, in Origin of the Earth and Moon, ed. R. M. Canup & K. Righter (Tucson: Univ. Arizona Press), 45
Hartmann, L., Calvet, N., Gullbring, E., & D'Alessio, P. 1998, ApJ, 495, 385
Hartmann, W. K., & Davis, D. R. 1975, Icarus, 24, 504
Hayashi, C. 1981, Prog. Theor. Phys. Suppl., 70, 35
Hayashi, C., Nakazawa, K., & Nakagawa, Y. 1985, in Protostars and Planets II, ed. D. C. Black & M. S. Matthew (Tucson: Univ. Arizona Press), 1100
Ida, S., Bryden, G., Lin, D. N. C., & Tanaka, H. 2000, ApJ, 534, 428
Ida, S., & Makino, J. 1993, Icarus, 106, 210
Ikoma, M., Nakazawa, K., & Emori, H. 2000, ApJ, 537, 1013
Iwasaki, K., Emori, H., Nakazawa, K., & Tanaka, H. 2002, PASJ, 54, 471
Jorissen, A., Mayor, M., & Udry, S. 2001, A&A, 379, 992
Kokubo, E., & Ida, S. 1995, Icarus, 114, 247
———. 1996, Icarus, 123, 180
———. 1998, Icarus, 131, 171
———. 2000, Icarus, 143, 15
———. 2002, ApJ, 581, 666
Koller, J., Li, H., & Lin, D. N. C. 2003, ApJ, 596, L91
Kominami, J., & Ida, S. 2002, Icarus, 157, 43
Lin, D. N. C., Bodenheimer, P., & Richardson, D. 1996, Nature, 380, 606
Lin, D. N. C., & Ida, S. 1997, ApJ, 477, 781
Lin, D. N. C., & Papaloizou, J. C. B. 1985, in Protostars and Planets II, ed. D. C. Black & M. S. Matthew (Tuscon: Univ. Arizona Press), 981
———. 1993, in Protostars and Planets III, ed. E. H. Levy & J. I. Lunine (Tucson: Univ. Arizona Press), 749
Lin, D. N. C., & Pringle, J. E. 1990, ApJ, 358, 515
Lissauer, J. J. 1987, Icarus, 69, 249
Lissauer, J. J., & Stewart, G. R. 1993, in Protostars and Planets III, ed. E. H. Levy & J. I. Lunine (Tucson: Univ. Arizona Press), 1061
Lynden-Bell, D., & Pringle, J. E. 1974, MNRAS, 168, 603
Marcy, G. W., Cochran, W. D., & Mayor, M. 2000, in Protostars and Planets IV, ed. V. Mannings, A. P. Boss, & S. S. Russell (Tucson: Univ. Arizona Press), 1285
Marzari, F., & Weidenschilling, S. 2002, Icarus, 156, 570

Matsuyama, I., Johnstone, D., & Murray, N. 2003, ApJ, 585, L143
Mizuno, H. 1980, Prog. Theor. Phys., 64, 544
Murray, N., & Chaboyer, B. 2002, ApJ, 566, 442
Murray, N., Hansen, B., Holman, M., & Tremaine, S. 1998, Science, 279, 69
Nakamoto, T., & Nakagawa, Y. 1994, ApJ, 421, 640
Papaloizou, J. C. B., & Lin, D. N. C. 1995, ARA&A, 33, 505
Papaloizou, J. C. B., & Terquem, C. 1999, ApJ, 521, 823
Patzold, M., & Rauer, H. 2002, ApJ, 568, L117
Podolak, M. 2003, Icarus, 165, 428
Pollack, J. B., Hubickyj, O., Bodenheimer, P., Lissauer, J. J., Podolak, M., & Greenzweig, Y. 1996, Icarus, 124, 62
Rafikov, R. R. 2003, AJ, 125, 922
Safronov, V. 1969, Evolution of the Protoplanetary Cloud and Formation of the Earth and Planets (Moscow: Nauka)
Santos, N. C., Israelian, G., & Mayor, M. 2001, A&A, 373, 1019
Shakura, N. I., & Sunyaev, R. A. 1973, A&A, 24, 337
Shang, H., Shu, F., Lee, T., & Glassgold, A. 2000, Space Sci. Rev., 92, 153
Shu, F. H., Johnstone, D., & Hollenbach, D. 1993, Icarus, 106, 92
Stevenson, D. J. 1982, Planet. Space Sci., 30, 755
Tabachnik, S., & Tremaine, S. 2002, MNRAS, 335, 151
Tanaka, H., & Ida, S. 1999, Icarus, 139, 350
Tanaka, H., Takeuchi, T., & Ward, W. R. 2002, ApJ, 565, 1257
Tanigawa, T., & Watanabe, S. 2002, ApJ, 580, 506
Terquem, C. 2003, MNRAS, 341, 1157
Thi, W. F., et al. 2001, Nature, 409, 60
Thommes, E. W., Duncan, M. J., & Levison, H. F. 2003, Icarus, 161, 431
Toomre, A. 1964, ApJ, 139, 1217
Trilling, D. E., Benz, W., Guillot, T., Lunine, J. I., Hubbard, W. B., & Burrows, A. 1998, ApJ, 500, 428
Trilling, D. E., Lunine, J. I., & Benz, W. 2002, A&A, 394, 241
Udry, S., Mayor, M., & Santos, N. C. 2003, A&A, 407, 369
Ward, W. 1986, Icarus, 67, 164
———. 1993, Icarus, 106, 274
———. 1997, Icarus, 126, 261
Weidenschilling, S., & Marzari, F. 1996, Nature, 384, 619
Wetherill, G. W. 1980, ARA&A, 18, 77
Wetherill, G. W., & Stewart, G. R. 1989, Icarus, 77, 330
Wuchterl, G., Guillot, T., & Lissauer, J. J. 2000, in Protostars and Planets IV, ed. V. Mannings, A. P. Boss, & S. S. Russell (Tuscon: Univ. Arizona Press), 1081
Wyatt, M. C., et al. 2003, MNRAS, 342, 876
Zucker, S., & Mazeh, T. 2002, ApJ, 568, L113